

DTIC FILE COPY

3

RADC-TR-89-144
In-House Report
October 1989



AD-A215 242

POLARIZATION RADAR PROCESSING TECHNOLOGY

Kenneth C. Stiefvater, Russell D. Brown, Vincent C. Vannicola, Michael C. Wicks

APPROVED FOR PUBLIC RELEASE; DISTRIBUTION UNLIMITED.

DTIC
ELECTE
NOV 21 1989
S B D

ROME AIR DEVELOPMENT CENTER
Air Force Systems Command
Griffiss Air Force Base, NY 13441-5700

89 11 21 008

This report has been reviewed by the RADC Public Affairs Office (PA) and is releasable to the National Technical Information Service (NTIS). At NTIS it will be releasable to the general public, including foreign nations.

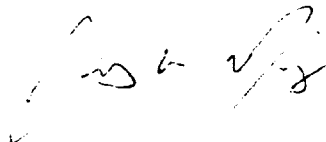
RADC TR-89-144 has been reviewed and is approved for publication.

APPROVED:



DANIEL R. MATTER, Capt, USAF
Acting Chief, Surveillance Technology Division
Directorate of Surveillance

APPROVED:



JAMES W. YOUNGBERG, Lt Col, USAF
Assistant Director
Directorate of Surveillance

FOR THE COMMANDER:



JOHN A. RITZ
Directorate of Plans and Programs

If your address has changed or if you wish to be removed from the RADC mailing list, or if the addressee is no longer employed by your organization, please notify RADC (OCTS) Griffiss AFB NY 13441-5700. This will assist us in maintaining a current mailing list.

Do not return copies of this report unless contractual obligations or notices on a specific document requires that it be returned.

UNCLASSIFIED

SECURITY CLASSIFICATION OF THIS PAGE

REPORT DOCUMENTATION PAGE				Form Approved OMB No. 0704-0188	
1a. REPORT SECURITY CLASSIFICATION UNCLASSIFIED			1b. RESTRICTIVE MARKINGS N/A		
2a. SECURITY CLASSIFICATION AUTHORITY N/A			3. DISTRIBUTION/AVAILABILITY OF REPORT Approved for public release; distribution unlimited.		
2b. DECLASSIFICATION/DOWNGRADING SCHEDULE N/A			5. MONITORING ORGANIZATION REPORT NUMBER(S) N/A		
4. PERFORMING ORGANIZATION REPORT NUMBER(S) RADC-TR-89-144			7a. NAME OF MONITORING ORGANIZATION Rome Air Development Center (OCTS)		
6a. NAME OF PERFORMING ORGANIZATION Rome Air Development Center		6b. OFFICE SYMBOL (If applicable) OCTS		7b. ADDRESS (City, State, and ZIP Code) Griffiss AFB NY 13441-5700	
6c. ADDRESS (City, State, and ZIP Code) Griffiss AFB NY 13441-5700		9. PROCUREMENT INSTRUMENT IDENTIFICATION NUMBER N/A		10. SOURCE OF FUNDING NUMBERS	
8a. NAME OF FUNDING/SPONSORING ORGANIZATION Rome Air Development Center		8b. OFFICE SYMBOL (If applicable) OCTS		10. SOURCE OF FUNDING NUMBERS	
8c. ADDRESS (City, State, and ZIP Code) Griffiss AFB NY 13441-5700		PROGRAM ELEMENT NO. 62702F		PROJECT NO. 4506	TASK NO. 11
				WORK UNIT 58	ACCESSION NO.
11. TITLE (Include Security Classification) POLARIZATION RADAR PROCESSING TECHNOLOGY					
12. PERSONAL AUTHOR(S) Kenneth C. Stiefvater, Russell D. Brown, Vincent C. Vannicola, Michael C. Wicks					
13a. TYPE OF REPORT In-House		13b. TIME COVERED FROM 1985 TO 1988		14. DATE OF REPORT (Year, Month, Day) October 1989	
				15. PAGE COUNT 68	
16. SUPPLEMENTARY NOTATION N/A					
17. COSATI CODES			18. SUBJECT TERMS (Continue on reverse if necessary and identify by block number)		
FIELD	GROUP	SUB-GROUP	Polarization Signal Processing		
17	09				
19. ABSTRACT (Continue on reverse if necessary and identify by block number)					
<p>A comprehensive effort is presented involving measurements and performance evaluation for the detection of scatters immersed in a background of natural and man-made clutter using polarization diverse waveforms. The effort spans evaluation from the initial stages of theoretical formulation to processor performance evaluation using real world data. The theoretical approach consists of determining polarimetric statistical properties of the backscatter waveform and the use of these properties to derive the optimum dual polarized S-Band radar system with selectable polarization on both transmit and receive. Recording equipment consists of 12 bit digital in-phase and quadrature channels indexed in time and phase for both polarizations. Several processors utilizing optimum and sub-optimum algorithms were evaluated using simulated and live radar data and performance results compared. The processor types include fully adaptive algorithms designed to operate on polarimetric spectral spread waveforms, and several combinations of single channel and polarization diverse receivers with both single and dual transmit polarization. A conventional fixed transmit (cont'd)</p>					
20. DISTRIBUTION/AVAILABILITY OF ABSTRACT <input checked="" type="checkbox"/> UNCLASSIFIED/UNLIMITED <input type="checkbox"/> SAME AS RPT. <input type="checkbox"/> DTIC USERS			21. ABSTRACT SECURITY CLASSIFICATION UNCLASSIFIED		
22a. NAME OF RESPONSIBLE INDIVIDUAL KENNETH C. STIEFVATER			22b. TELEPHONE (Include Area Code) (315) 330-4437		22c. OFFICE SYMBOL RADC(OCTS)

UNCLASSIFIED

19. (Cont'd). and receive mode with no spectral processing is included. Comparisons are made between the various processors. The simulated and real data consist of randomly scattered dipoles, spheres, Swerling type scatters, and scatters of opportunity. Results are plotted and evaluated by displaying probability of detection as a function of signal-to-noise ratio with processor type as a parameter.

RRH #
UNCLASSIFIED

TABLE OF CONTENTS

1.0	INTRODUCTION	1
2.0	THEORY	5
3.0	APPROACH	18
3.1	DATA COLLECTION	18
3.2	DATA REDUCTION	25
3.3	PROCESSING ALGORITHMS	26
3.4	PROCESSOR EVALUATION	30
4.0	EXPERIMENTAL RESULTS	41
5.0	CONCLUSIONS	55
6.0	REFERENCES	56

Accession For	
NTIS GRA&I	<input checked="" type="checkbox"/>
DTIC TAB	<input type="checkbox"/>
Unannounced	<input type="checkbox"/>
Justification	
By	
Distribution/	
Availability Codes	
Dist	Avail and/or Special
A-1	

LIST OF FIGURES

Figure 1	Polarization Modulation Receiver	13
Figure 2	S-Band Radar at RADC	20
Figure 3	Experiment Block Diagram	21
Figure 4	Equipment Configuration	21
Figure 5	Three Polarization Receiver/Processors	25
Figure 6	Optimum Matrix Method Processing Algorithm	31
Figure 7	Block Diagram of Vector Weighting Simulation	31
Figure 8	Horizontal Transmit Polarization CNR=-20dB	35
Figure 9	Vertical Transmit Polarization CNR=-20dB	35
Figure 10	Horizontal Transmit Polarization CNR=10dB	36
Figure 11	Vertical Transmit Polarization CNR=10dB	36

Figure 12	Horizontal Transmit Polarization	37
	CNR=30dB	
Figure 13	Vertical Transmit Polarization	37
	CNR=30dB	
Figure 14	Pulse Compressed Target Data (HH)	38
Figure 15	Pulse Compressed Clutter Data (HH)	38
Figure 16	Pulse Compressed Target Data (HV)	39
Figure 17	Pulse Compressed Clutter Data (HV)	39
Figure 18	Target Spectrum (HV)	40
Figure 19	Clutter Spectrum (HV)	40
Figure 20	Uncompressed Target And Clutter Data	43
	I Channel Versus Range	
Figure 21	Uncompressed Target And Clutter Data	44
	Three Second Delay From Fig 20	
Figure 22	Pulse Compressed Target And	46
	Clutter Data Magnitude Versus Range	
Figure 23	Pulse Compressed Target And Clutter	47
	Data Three Second Delay From Fig 22	

Figure 24	Range Doppler 3D Plot Of Aircraft/Chaff	50
Figure 25	Horizontal Transmit Polarization CNR=-20dB	52
Figure 26	Vertical Transmit Polarization CNR=-20dB	52
Figure 27	Horizontal Transmit Polarization CNR=10dB	53
Figure 28	Vertical Transmit Polarization CNR=10dB	53
Figure 29	Horizontal Transmit Polarization CNR=30dB	54
Figure 30	Vertical Transmit Polarization CNR=30dB	54

LIST OF TABLES

Table 1	Key To Curves Of PD Plots	32
---------	---------------------------	----

1. INTRODUCTION

Future radar signal processing techniques must use doppler and polarization processing to discriminate between targets and interfering clutter and chaff. Target and clutter scatterers have characteristic range, doppler and polarization properties which provide for enhanced target detection performance compared to conventional single channel matched filter receivers. This is due to the fact that additional target and background discriminants are available in dual channel polarization sensitive systems.

The scattering centers of radar targets and clutter often have preferred spatial orientations and thus selectively scatter radar signals according to the orientation of the incident electric field. In order to accurately model radar targets or clutter, it is necessary to consider their polarization properties in terms of a complex scattering matrix, which represents a scatterer's response to two orthogonal incident polarizations. By considering time and range varying matrix elements, the scattering matrix provides a means for jointly modeling a scatterer's doppler and range dependent polarization characteristics.

This paper provides a brief review of basic radar polarization theory [1], including a discussion of the use of the polarization scattering matrix in systems analysis. Theoretical stochastic doppler and polarization target and clutter models are also discussed, and the optimum receiver is formulated [2]. Two forms of the Optimum Matrix Method [3] approximation to the optimum receiver are presented and evaluated using experimental and simulated results, illustrating receiver performance for the detection of desired targets in clutter.

Polarization discrimination can be exploited via three significantly different concepts which may be introduced by analogy to doppler processing. In the doppler domain the three concepts are embodied as delay line cancellers, optimum doppler filter banks with

prespecified transmit waveforms, and doppler filter banks with adaptive transmit waveforms.

Thus, for a delay line canceller, the design procedure is to build a receive filter that has a null at the center frequency of the clutter spectrum. A priori knowledge of the target doppler characteristics are not factored into the design of the delay line canceller. However, the design of an optimum doppler filter bank depends upon both the target's doppler frequency and the clutter spectrum. Specifically, each receive filter peaks at a different preassigned doppler frequency corresponding to an expected target doppler. Although each filter of the bank has high response only to a small range of target doppler, the entire bank has high response to all possible target doppler frequencies. The preceding discussion of the two processors has assumed that the transmit waveform consists of a constant interpulse period pulse train where each pulse has the same amplitude and phase. Thus, as an example, a two pulse canceller subtracts and cancels successive returns from a zero velocity point target since the returns have equal amplitude and phase. However, they have the same amplitude and phase only when the two sequential transmitted pulses are identical. The third type of doppler processor adaptively controls the transmitted signal characteristics to further improve performance. When the amplitude and phase of each transmitted pulse can be varied, the receiver may be designed to account for this particular waveform, and the resulting target doppler and clutter spectrum. It has been shown that superior target detection performance is obtained via joint optimization of the transmit waveform together with the receive filter, as compared to optimization of the receive filter alone. As the joint optimization depends upon the clutter/chaff doppler characteristics, the technique is doubly adaptive. Both the transmit waveform and the receive filter are adaptive to optimize the doppler discrimination between target and clutter.

Similarly for the polarization domain, there are canceller type processors that are designed to have zero response at the average polarization of the clutter/chaff and whose design does not incorporate any a priori knowledge of the polarization characteristics of the targets. In addition, there is an adaptive receiver to enhance the discrimination between target and clutter/chaff when the transmit polarization is prespecified. These two techniques are compatible with doppler processing. Thus, polarization processing and adaptive or non-adaptive doppler processing may be cascaded to gain more effective discrimination between targets and clutter/chaff. Finally, an adaptive technique can be configured with both the transmit polarization and receive polarization adaptable. This can be configured as dual domain adaptivity by simultaneously adapting in the polarization and doppler domains. This last procedure is the most powerful way of using the two domains for discriminating between targets and clutter/chaff.

The goal is to improve target detectability and to determine the benefits that can be accrued when the polarization and doppler domains are fully exploited. In order to determine this, it was necessary to assemble data to establish the characteristics of targets and clutter/chaff. This data base was used to evaluate the absolute and relative target detection capabilities of a number of signal processing algorithms. A particularly successful algorithm was a matrix method of jointly optimizing the transmit waveform polarization, the receive polarization, and the doppler filter. This technique outperformed all other approaches studied.

The matrix approach is a computationally complex procedure which involves simultaneous optimization of the joint polarization/doppler domain. A second, simplified technique, is one that uses sequential optimization of the disjoint polarization and doppler domains. Thus, polarization optimization can be accomplished by using a canceller concept based on either polarization nulling, polarization eigenanalysis, or receive polarization

orthogonality. After adaptive polarization processing, the doppler filtering may be performed subsequently. Other processors of interest for performance comparison are based upon fixed polarization systems using non-coherent or coherent doppler processing. These provide a reference to determine the additional processing gain obtained by the optimum combined polarization-doppler processor over conventional radar processing methods.

The radar backscatter environment has stochastic characteristics associated with doppler, range, and electromagnetic scattering phenomena. The environment consists of target and clutter scatterers, each having characteristic doppler, range and polarization properties. In optimization theory, Van Trees [1] uses analytical approaches to solve a set of integral equations for the design of a radar system optimized over a set of radar environmental factors. This factors include the effects of the clutter scattering function on the incident transmitted waveform. Such a scattering function is directly related to an autocovariance function of the noise resulting from the backscattered clutter with the transmitted incident waveform factored out. Such a function for a single-channel system incorporates all the statistics one needs to know about the doppler and range spread characteristics of the environment in order to optimize the radar. For a multiple channel system, the transmit waveform is a vector, and the scattering function is a tensor. This has been indicated by several investigators [2,3] where the parameters within the tensor were time averaged, but doppler and range spread correlation were not considered. In the latter [3], the author indicates that the benefits can be obtained with respect to the target discrimination by controlling the transmitted polarization waveform and receiver in such a manner as to take advantage of the degree of coherence of the signals in the receiver channels. There have been many papers on these subjects. Stochastic models [4] describing the spectral and polarization characteristics of radar echoes from chaff clouds consisting of rotating dipoles with completely random or preferred orientations have been

used. Other papers [5,6] include modeling and polarization processing with optimum transmit waveform vectors for the enhancement of target detection in clutter. These approaches utilize radar scattering matrix properties in the design of a two-channel vector receiver which discriminates between the scattering matrix range-doppler spread characteristics of the target and those of the clutter. Computer simulations were performed [5] to verify some simplified mathematical models.

2. THEORY

This section provides the analytical development, basic mathematical expressions, and their justification, derived from stochastic processes and optimum filter theory. The goal is the design of the optimum system, making use of the two channel polarization and range-doppler spread scatterer properties. This approach is an extension of the development presented by Van Trees [1] for the single channel case.

A radar backscatter environment can be represented by a statistically time varying and range varying polarization scattering matrix [7]. The model is general and can be used for the clutter as well as the target. Once the targets are specified, the radar design can be optimized. Performance of the system can also be evaluated. The procedures for system design and performance evaluation are extensions of widely accepted optimum filter design theory. The primary difference is that the target model to which the procedures are applied is a scattering matrix random process. In addition to serving as design criteria for the radar system, such a model also designates the required field measurements for completely specifying such a scatterer. As a consequence of this model, an approach for the generalized ambiguity function of multiple channel systems is introduced. These discriminants between the target and the clutter will provide a new dimension for

improving target detection in a real-world clutter environment.

First, we review target modeling and system optimization for the single channel radar system. Using the review as a basis, we will extend the treatment of the multiple channel system specialized for the polarization case. The procedures for deriving the target model, the optimum transmit waveform, and the optimum receiver for the single channel case, or single polarization sense, are given as follows:

The signal received by the radar, $\tilde{r}(t)$, from a slowly fluctuating point target in a clutter environment is

$$\tilde{r}(t) = \tilde{b} \tilde{f}_d(t) + \tilde{n}_c(t) + \tilde{w}(t), \quad H_1 \quad (1)$$

$$\tilde{r}(t) = \tilde{n}_c(t) + \tilde{w}(t), \quad H_0 \quad (2)$$

where:

- H_1 hypothesis target present, H_0 target absent
- $\tilde{f}_d(t)$ is the complex range delayed doppler shifted replica of the transmit waveform $\tilde{f}(t)$
- \tilde{b} is a complex random variable and represents the target backscatter, propagation losses, and antenna responses
- $\tilde{n}_c(t)$ is the received signal from the clutter and is a complex random process
- $\tilde{w}(t)$ is the additive white noise in the receiver.

The tilde \sim designates the complex low-pass equivalent of the radar signal.

The received signal from the clutter is the convolution of the clutter with the transmit waveform. Convolution is with respect to the range variable λ .

$$\tilde{n}_c(t) = \sqrt{E_t} \int_{-\infty}^{\infty} \tilde{f}(t - \lambda) \tilde{b}(t - \frac{\lambda}{2}, \lambda) d\lambda \quad (3)$$

E_t is the energy in the transmitted waveform.

$\tilde{n}_c(t)$ is a zero-mean complex Gaussian random process with the covariance function:

$$\tilde{K}_{\tilde{n}_c}(t, u) = E_t \int_{-\infty}^{\infty} \tilde{f}(t - \lambda) \tilde{K}_{DR}\{t - u\} \tilde{f}^*(u - \lambda) d\lambda \quad (4)$$

$$= E_t \iint_{-\infty}^{\infty} \tilde{f}(t - u) \tilde{S}_{DR}\{\nu, \lambda\} \tilde{f}^*(u - \lambda) e^{j 2\pi\nu(t-u)} d\nu d\lambda \quad (5)$$

where the correlation function, $\tilde{K}_{DR}\{\tau, \lambda\}$, is a two-variable function that depends on the reflective properties of the target, and $\tilde{S}_{DR}\{\nu, \lambda\}$ represents the spectrum of the process $\tilde{b}(t, \lambda)$ and is called the scattering function of the clutter. The two functions are a Fourier Transform pair. The white noise $\tilde{w}(t)$ is likewise a complex Gaussian random process but with covariance function $\tilde{K}_{\tilde{w}}(t, u) = N_0 \delta(t - u)$.

The conventional receiver is designed for detecting a target in white noise only. We compute the sufficient statistic $\tilde{\ell}$:

$$\tilde{\ell} \triangleq \int_{-\infty}^{\infty} \tilde{r}(t) \tilde{f}^*(t - \tau_d) e^{-j \omega_d t} dt \quad (6)$$

and make the threshold comparison test:

$$|\tilde{\ell}|^2 \underset{H_0}{\overset{H_1}{\geq}} \gamma \quad (7)$$

The output (S/N) is Δ_{ω_o} given by:

$$\Delta_{\omega_o} = \frac{\bar{E} / N_o}{1 + \rho_r} \quad (8)$$

$$\Delta_{\omega_o} = \frac{\bar{E}_r / N_o}{1 + (E_t / N_o) \iint_{-\infty}^{\infty} d\nu d\lambda \tilde{S}_{DR}\{\nu, \lambda\} \theta\{\tau_d - \lambda, \nu - f_d\}} \quad (9)$$

- ρ_r represents the degradation due to the clutter
 $f(t)$ is the transmit waveform which is used here as a modulation or filter function
 τ_d is the target round trip delay
 ω_d is the target doppler frequency
 γ is a predetermined threshold
 \bar{E}_r is the average energy received from the target
 \bar{E}_t is the transmit energy
 N_o is the white noise energy (kT)
 $\theta\{\lambda, \nu\}$ is the waveform ambiguity function

The optimum single-channel receiver is designed for detecting a target in clutter as well as white noise. The optimum receiver computes

$$\mathcal{L} \triangleq \int_{-\infty}^{\infty} \tilde{r}(t) \tilde{g}^*(t) dt \quad (10)$$

where $g(\cdot)$ satisfies the integral equation

$$\tilde{f}(t - \tau_d) e^{j\omega_d t} = E_t \iint_{-\infty}^{\infty} \tilde{f}(t - \lambda) \tilde{K}_{DR}(t - u, \lambda) \tilde{f}^*(u - \lambda) \tilde{g}(u) du d\lambda + N_o \tilde{g}(t) \quad (11)$$

The function $\tilde{g}(\cdot)$ is a modulation or filter function and is used in place of $\tilde{f}(\cdot)$ when colored noise is present. The performance is obtained by evaluating

$$\Delta = \bar{E}_r \iint_{T_i}^{T_f} \tilde{f}(t) \tilde{Q}_n^*(t, u) \tilde{f}^*(u) dt du \quad (12)$$

$$\Delta = \bar{E}_r \int_{T_i}^{T_f} \tilde{f}(t) \tilde{g}^*(t) dt \quad (13)$$

where the inverse Kernel $\tilde{Q}_n(t, u)$ satisfies

$$\int_{T_i}^{T_f} \left[\tilde{K}_{n_c}(t, z) + N_o \delta(t-z) \right] \tilde{Q}_n(z, u) dz = \delta(t-u) \quad (14)$$

Then the false alarm and detection probability are related by

$$P_{FA} = (F_D)^{1+\Delta} \quad (15)$$

For certain special conditions of the scattering function we can simplify equations (10) and (11) further. The optimal waveform, $\tilde{f}_o(t)$, must satisfy [1] the following integral equation

$$\int_{T_i}^{T_f} \tilde{h}_{ou}(t, u) \tilde{f}_o(u) du + \lambda_E \tilde{f}^*(t) - \lambda_B \tilde{f}_o(t) = 0 \quad (16)$$

where $\tilde{h}_{ou}(t, u)$ is the optimum unrealizable filter satisfying the equation

$$N_o \tilde{h}_{ou}(t, u) + \int_{T_i}^{T_f} \tilde{h}_{ou}(x, u) \tilde{K}_{n_c}(t, x) dx = \tilde{K}_{n_c}(t, u) \quad (17)$$

$$T_i \leq t, u \leq T_f$$

λ_E and λ_B are LaGrange multipliers with an energy and bandwidth constraint.

When we transmit and receive over two channels as we do in the dual polarization case, the received signals given in Equations (1) and (2) become two-element vectors

$$\tilde{\mathbf{r}}(t) = \tilde{\mathbf{b}} \mathbf{f}_d(t) + \tilde{\mathbf{n}}_c(t) + \tilde{\mathbf{w}}(t) \quad H_1 \quad (18)$$

$$\tilde{\mathbf{r}}(t) = \tilde{\mathbf{n}}_c \tilde{\mathbf{w}}(t) \quad H_0 \quad (19)$$

where boldface variables denote vectors of the polarization components. The vector received signal, $\tilde{\mathbf{r}}(t)$, contains a component from each receive polarization channel.

The scattering matrix, $\tilde{\mathbf{b}}(t)$, contains four components: the vertically polarized scattering of the incident vertically polarized energy (VV), the cross polarized components (VH and HV), and the horizontal scattering component (HH). The scattering is modeled as a slowly

fluctuating point target with zero mean complex Gaussian random elements. In general, the scattering components \tilde{b}_{VH} and \tilde{b}_{HV} may be assumed to be equal. $\tilde{f}_d(t)$ is the time delayed doppler shifted replica of the transmit waveform vector with transmit energy E_t . The receiver noise, $\tilde{w}(t)$, is a vector with white noise components, $\tilde{w}_V(t)$ and $\tilde{w}_H(t)$, which are independent for the two polarization channels. The colored noise vector due to backscatter from clutter, $\tilde{n}_c(t)$, also contains dual polarization components which are obtained by convolving the range-doppler variant scattering matrix of the clutter process,

$$\tilde{b}(t - \frac{\lambda}{2}, \lambda) \triangleq \begin{bmatrix} \tilde{b}_V^T(t - \frac{\lambda}{2}, \lambda) \\ \tilde{b}_H^T(t - \frac{\lambda}{2}, \lambda) \end{bmatrix} \triangleq \begin{bmatrix} \tilde{b}_{VV}(t - \frac{\lambda}{2}, \lambda) & \tilde{b}_{VH}(t - \frac{\lambda}{2}, \lambda) \\ \tilde{b}_{HV}(t - \frac{\lambda}{2}, \lambda) & \tilde{b}_{HH}(t - \frac{\lambda}{2}, \lambda) \end{bmatrix} \quad (20)$$

with the transmit vector,

$$\tilde{f}(t) = \begin{bmatrix} \tilde{f}_V(t) \\ \tilde{f}_H(t) \end{bmatrix} \quad (21)$$

which is normalized to unit energy. The scattering matrix $\tilde{b}(t - \frac{\lambda}{2}, \lambda)$, a zero mean Gaussian random process, interacts with the transmit waveform resulting in

$$\tilde{n}_c(t) = \begin{bmatrix} n_{cV}(t) \\ n_{cH}(t) \end{bmatrix} = \sqrt{E_t} \int_{-\infty}^{\infty} \tilde{b}(t - \frac{\lambda}{2}, \lambda) f(t - \lambda) d\lambda \quad (22)$$

This expression represents the colored noise vector due to backscatter from the clutter, where t is time and λ is radar range expressed in units of time. It can be shown that the clutter vector covariance function is a matrix

$$\tilde{\mathbf{K}}_{\mathbf{n}_c}(t,u) \triangleq E\{\tilde{\mathbf{n}}_c(t) \tilde{\mathbf{n}}_c^\dagger(u)\} = \begin{bmatrix} \tilde{\mathbf{K}}_{\mathbf{n}_c}^{VV}(t,u) & \tilde{\mathbf{K}}_{\mathbf{n}_c}^{VH}(t,u) \\ \tilde{\mathbf{K}}_{\mathbf{n}_c}^{HV}(t,u) & \tilde{\mathbf{K}}_{\mathbf{n}_c}^{HH}(t,u) \end{bmatrix} \quad (23)$$

Substituting $\tilde{\mathbf{n}}_c(t)$ into (23) and assuming the returns from different range intervals are statistically independent and that the return from each interval is a sample vector function of a stationary zero-mean Gaussian random process,

$$\tilde{\mathbf{K}}_{\mathbf{n}_c}(t,u) = E_t \int_{-\infty}^{\infty} \tilde{\mathbf{f}}^T(t-\lambda) \tilde{\mathbf{K}}_{\text{DR}}\{t-u, \lambda\} \tilde{\mathbf{f}}^*(u-\lambda) d\lambda \quad (24)$$

$$= E_t \iint_{-\infty}^{\infty} \tilde{\mathbf{f}}^T(t-\lambda) \tilde{\mathbf{S}}_{\text{DR}}\{\nu, \lambda\} \tilde{\mathbf{f}}^*(u-\lambda) e^{j2\pi\nu(t-u)} d\nu d\lambda \quad (25)$$

The tensor correlation function $\tilde{\mathbf{K}}_{\text{DR}}\{\tau, \lambda\}$ is a two-variable fourth-rank tensor that depends on the reflective properties of the clutter. The 'DR' subscript denotes that the clutter is doubly spread in both doppler and range. The function $\tilde{\mathbf{S}}_{\text{DR}}\{\nu, \lambda\}$ is a two-variable, fourth-rank tensor representing the spectrum of the process, and is related to $\tilde{\mathbf{K}}_{\text{DR}}(\tau, \lambda)$ by the Fourier transform

$$\tilde{\mathbf{K}}_{\text{DR}}(\tau, \lambda) = \int_{-\infty}^{\infty} \tilde{\mathbf{S}}_{\text{DR}}(\nu, \lambda) e^{j2\pi\nu\tau} d\nu \quad (26)$$

It can be called the tensor scattering function of the process $\tilde{\mathbf{b}}(\tau, \lambda)$. $\tilde{\mathbf{K}}_{\text{DR}}(\tau, \lambda)$ provides 16 different elements (discriminants) when one considers the statistical behavior of the polarization random process scattering matrix. Assuming the scattering matrix is a non-negative Hermitian process, then the number of independent elements reduces to 10, which still provides a wide selection of polarization/doppler discriminants. These tensor

element functions completely describe the clutter irrespective of the transmit waveform and receiver design. They can be used in the waveform and receiver optimization as well as the performance equations in the same sense that the scalar correlation and scattering functions are used in the design equations of the single channel system.

The conventional receiver is one which is optimized for a signal corrupted by white noise instead of the clutter colored noise. In this case, the optimum filter is a vector matched filter. The sufficient statistic computed by the conventional receiver is,

$$\tilde{\ell} \triangleq \int_{-\infty}^{\infty} \tilde{\mathbf{r}}^T(t) \tilde{\mathbf{f}}^*(t - \tau_d) e^{-j\omega_d t} dt \quad (27)$$

and is compared to a threshold as in equation (7). The performance degradation is given by equation (9). For the vector case, we leave the ambiguity function in tensor/integral form.

$$\rho_r(\tau_d, \omega_d) = \frac{E_t}{N_o} \iiint \tilde{\mathbf{f}}^T(t - \tau_d) \tilde{\mathbf{f}}^T(t - \lambda) e^{j(\omega - \omega_d)t} \tilde{S}_{DR}(\nu, \lambda) \tilde{\mathbf{f}}^*(u - \lambda) \tilde{\mathbf{f}}(u - \tau_d) e^{-j(\omega - \omega_d)u} dt du d\lambda d\nu \quad (28)$$

Equation (28) introduces another model, that of the ambiguity function for the multi-channel case. It takes on a form suggested by the integral of the outer product of all the transmit vectors \mathbf{f} in equation (28).

In equation (9), the integral contained the waveform ambiguity function $\theta\{\tau_d - \lambda, \nu - \nu_d\}$. Equation (28) generalizes this function for the multi-channel case and contains the necessary functions and integrals to constitute an ambiguity function. However, it involves outer products with waveform vectors. The optimum receiver computes

$$\tilde{\ell} \triangleq \int_{-\infty}^{\infty} \tilde{r}^T(t) \tilde{g}^*(t) dt \quad (29)$$

for the vector case, and makes a threshold comparison as cited in equation (7).

A block diagram of the optimum receiver is given in Figure 1.

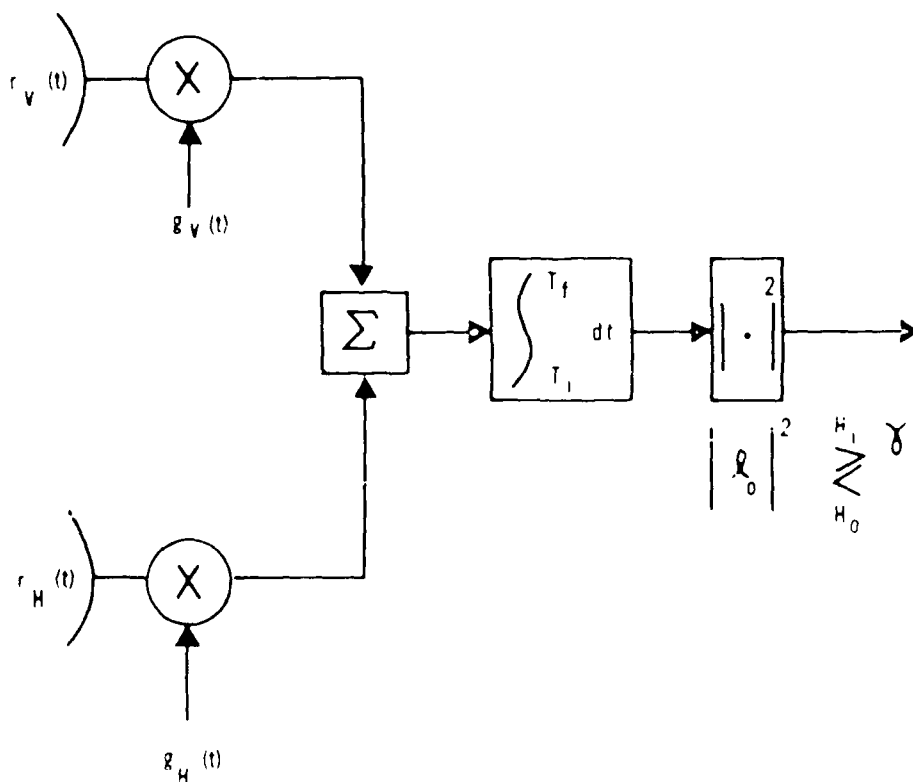


Figure 1. Polarization Modulation Receiver

$\tilde{g}(\cdot)$ satisfies the matrix equation:

$$\tilde{f}_d(t) = \int_{-\infty}^{\infty} \tilde{K}_{n_c}^{\sim}(t,u) \tilde{g}(u) du + N_o \tilde{g}(t) \quad (30)$$

$$= \iint_{-\infty}^{\infty} \tilde{f}^T(t-\lambda) \tilde{K}_{DR}(t-u, \lambda) \tilde{f}^*(u-\lambda) \tilde{g}(u) du d\lambda + N_o \tilde{g}(t) \quad (31)$$

The performance (output signal to noise ratio) of the optimum receiver is specified by

$$\Delta = E_r \iint_{T_i}^{T_f} \tilde{f}_d(t) \tilde{Q}^*(t,u) \tilde{f}^*(u) dt du \quad (32)$$

$$= E_r \int_{T_i}^{T_f} \tilde{f}_d^T(t) \tilde{g}^*(t) dt \quad (33)$$

The average energy received from the target is

$$E_r = E \left\{ \int_{-\infty}^{\infty} \tilde{S}^T(t) \tilde{S}^*(t) dt \right\} E_t \quad (34)$$

where $\tilde{S}(t) = \tilde{b}_f(t)$.

This reduces to

$$E_r = 2(\sigma_{VV}^2 + \sigma_{HV}^2) E_{tV} + 2(\sigma_{HH}^2 + \sigma_{VH}^2) E_{tH} + 4 \sqrt{E_{tV} E_{tH}} \operatorname{Re} \left\{ \rho_t (\sigma_{VV,VH}^2 + \sigma_{HV,HH}^2) \right\} \quad (35)$$

where σ_{VV}^2 is the variance of the b_{VV} element in the target scattering matrix and $\sigma_{VV,VH}^2$ is the covariance between the b_{VV} and the b_{VH} elements of the target scattering matrix. E_{tV} and E_{tH} are the transmit energy of the vertical channel and the

horizontal channel, respectively. ρ_t is the correlation coefficient between the vertical and horizontal waveforms.

The quantity Δ for which expressions have been given throughout this discussion is used to relate the detection and false alarm probability

$$P_F = (P_D)^{1+\Delta} \quad (36)$$

The above optimization procedures involve integral and tensor equations which are very difficult to solve analytically. In general even the scalar case is not trivial. Numerical methods applicable to computer approximations of these functions are valuable in approaching the optimum performance.

The extension of the waveform design case to the polarization channels involves vectors, matrices, and tensors in equations (16) and (17). The optimum unrealizable filter, \tilde{h}_{ou} , is a 2×2 matrix. The optimum waveform, \tilde{f}_o is a vector, and the autocorrelation function, \tilde{K}_{nc} is a matrix. It is important to note that the autocovariance matrix contains factors of the waveform vectors as defined in equation (24). Consequently, the filter must satisfy the equation

$$N_o \tilde{h}_{ou}(t,u) = E_t \int_{T_i}^{T_f} \int_{-\infty}^{\infty} \tilde{f}_o^T(t-\lambda) \tilde{K}_{DR}\{t-x,\lambda\} \tilde{f}_o^*(x-\lambda) [I\delta(x-u) - \tilde{h}_{ou}(x,u)] d\lambda dx \quad (37)$$

and the optimal waveform vector must satisfy the integral equation

$$\int_{T_i}^{T_f} \tilde{h}_{ou}(t,u) \tilde{f}_o(u) du + \lambda_E \tilde{f}_o(t) - \lambda_B \tilde{f}_o(t) = 0 \quad (38)$$

The energy and bandwidth constraints become

$$\int_{T_i}^{T_f} \tilde{\mathbf{f}}^T(t) \tilde{\mathbf{f}}^*(t) dt = 1 \quad (39)$$

and

$$\int_{T_i}^{T_f} \tilde{\mathbf{f}}(t) \tilde{\mathbf{f}}(t) dt = B^2 \quad (40)$$

We have extended the statistical model of a scatterer illuminated and observed on one channel to suit the two-channel polarization case. In that model we have accounted for the statistical range and doppler spread characteristics. The mathematical formulation for the polarization sensitive scatterer was written in the framework of a random process scattering matrix whose covariance properties took on a sixteen element tensor form. This tensor contained all the backscatter information necessary to determine the range/time/polarization dependent behavior of the received signal for any arbitrary transmit polarized waveform.

From such an analytical model, we extended the conventional (matched filter) processor, as well as the optimum receiver to include the polarization case. We produced an expression for the performance of the extended processor. In the extended processor case, the receiver contains vector channels, each having its own filter or modulating function determined from the time/range statistical properties of the transmit polarization waveform reacting with the clutter/target model. We also gave an expression which an optimal transmit waveform must satisfy for the polarization case.

Other approaches have been taken for the optimal processing of polarimetric received signals. Mohrhotra [8] decomposes the return signal into a complete orthonormal (C.O.N.)

set of eigenvalues. He develops all the associated processing in a similar manner as developed in this paper with an additional stage constituting signal and channel weights as functions of the eigenvalues. Each weight is applied to the channel in which the received signal has been correlated with its associated eigenvector function.

An optimum receiver which correlates the received signal $\tilde{r}(t)$ with $\tilde{g}(t)$, the vector modulation function, requires exact knowledge of the scattering statistics of the clutter for optimality. Since, in practice, only a numerical approximation of the clutter covariance matrix is available, and this information is obtained by a limited time observation of the clutter itself, a linearization of the optimum receiver suffices to compute detection probability versus signal-to-noise ratio for a selected false alarm probability. A further simplification is imposed by high power transmitter design, which favors the use of waveforms with uniform amplitude characteristics.

The receiver/processor implemented in the RADC Surveillance Laboratory, called the Optimum Matrix Method (OMM), follows the foregoing approach. Based on joint diagonalization of the target and clutter covariance matrices, OMM provides maximum separation of the target and clutter vector components in the processed output, prior to hypothesis testing. The method includes transmit vector waveform optimization derived from estimated target and clutter statistics. An efficient waveform design technique has been developed [5] which selects a most nearly optimum candidate from an assembled library of constrained transmit waveforms. Four other receivers and processing techniques, exhibiting various degrees of polarization and doppler adaptivity, have been evaluated in several experiments for comparison with the OMM, and are detailed in section 3.4.

3.0 APPROACH

This section covers the processor evaluation which includes experimental as well as simulated data utilized to predict the detection performance of various algorithms. Performance is measured in terms of probability of detection (PD) versus signal-to-noise ratio (SNR) as a function of clutter-to-noise ratio (CNR). The effort was divided into three areas: data collection, data reduction, and processor evaluation.

3.1 DATA COLLECTION

The experimental data sets were obtained using the S-Band, dual polarized tracking radar testbed located at Rome Air Development Center (RADC), in Rome, New York. The RF transmitting and receiving equipment, and antenna, are located on a 65 foot tower adjacent to the RADC Surveillance Laboratory, as shown in Figure 2. The antenna features an elevation over azimuth pedestal configuration which provides monopulse tracking and variable polarization. The main central horn is dual polarized for transmitting and receiving. Two independent S-Band channels are available on transmit and receive. On receive, the two orthogonally polarized channels are synchronously recorded and processed independently. The system has two transmitters, one for each polarization channel. This approach has the advantages of independent frequency capability, polarization versatility, and increased power, relative to a single transmitter configuration. Transmit polarization agility may be achieved at low power levels by controlling the signal inputs to the two transmitters. A wideband mode is available for the S-Band waveform generation and processing systems which allows signal bandwidths of up to 320 MHz to be utilized.

The S-Band radar system parameters are as follows:

System:

Frequency	3.1 - 3.7 GHz
Peak Power	170 Kilowatts
Average Power	15 Kilowatts
Pulse Width	Up to 200 usec (max)
PRF	Up to 5000 pps (max)
Dynamic Range	+90dB in 1MHz bandwidth
Data Channels	Four: Two I, Two Q

Cassegrain Feed:

Polarization	Five Horn Cassegrain Sum and Error Horns - Linear
Isolation	30dB between vertical and horizontal
Tracking Null	30dB between difference and sum channels

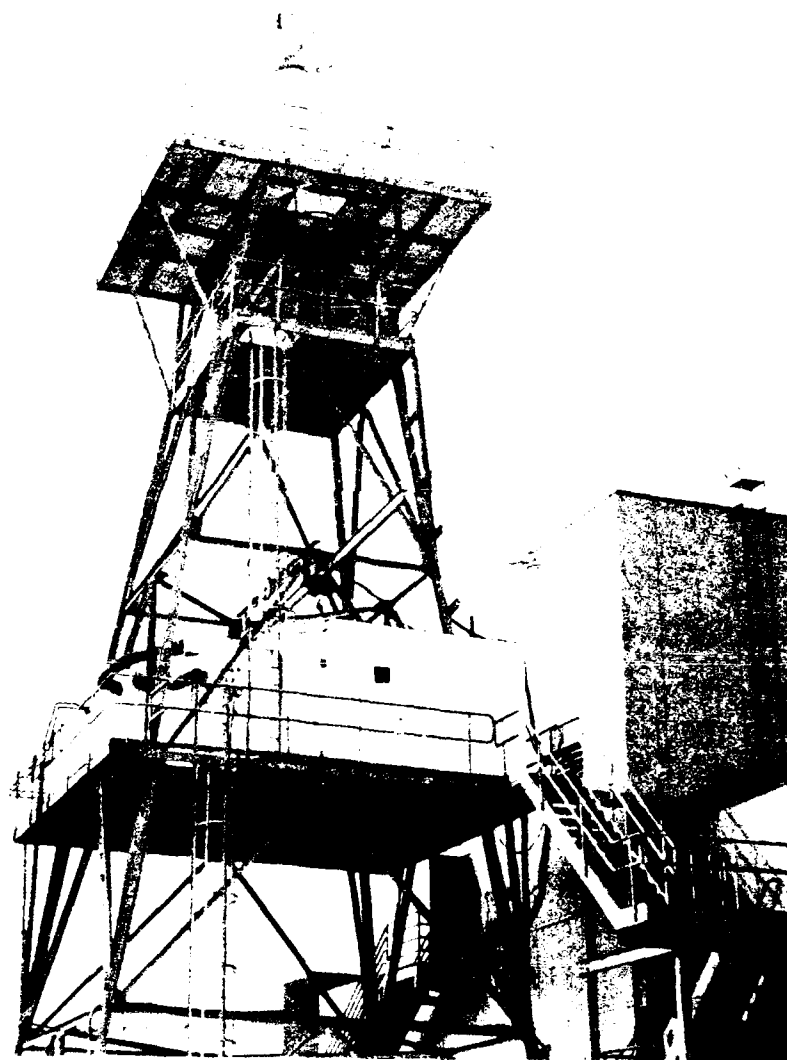


Figure 2. S-Band Radar at RADC

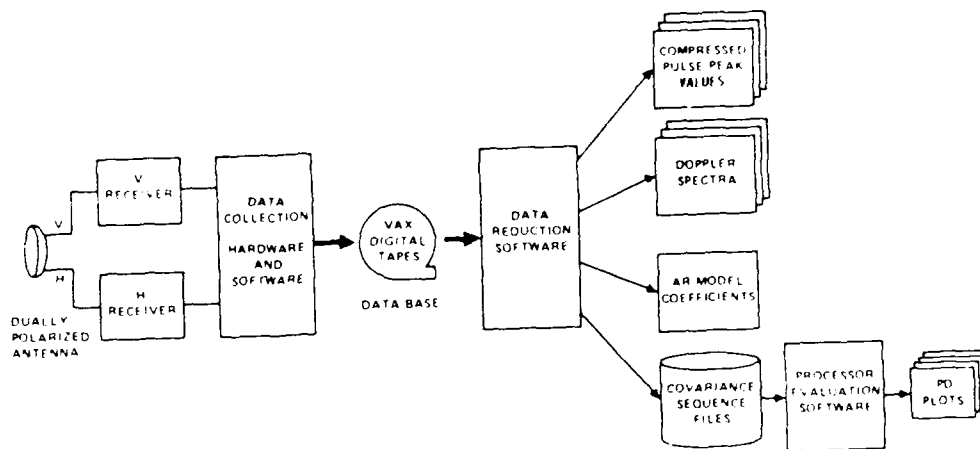


Figure 3. Experiment Block Diagram

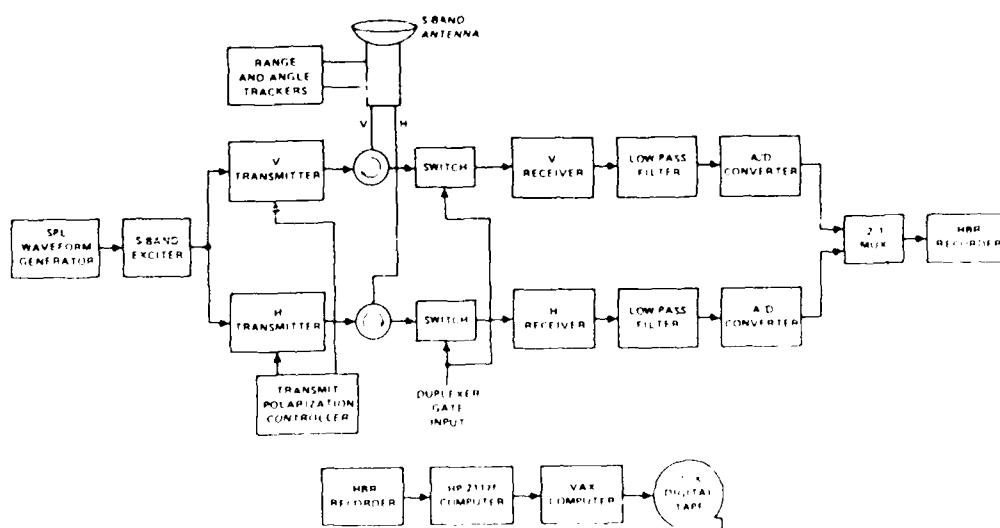


Figure 4. Equipment Configuration

Antenna:

Gain	42dB for main channel 23dB for monopulse channel
Dish Diameter	20 feet
Sidelobes	Elevation and Azimuth, 1st and 2nd sidelobes 20dB below main. 3rd is 25dB below main.
Focus to Diameter	0.4
Azimuth Travel	720° (wrap limited)
Elevation Travel	-5° to 185°

The data collection activity consisted of recording dual-polarized returns from targets and clutter using the S-Band system. Figure 3 is the experiment block diagram. The S-Band antenna provided independent outputs for the horizontal (H) and vertical (V) receive channels. Both channels were synchronously detected by the receivers whose baseband outputs were digitized using 12 bit analog to digital converters. The A/D converter outputs were buffered and transcribed to VAX-compatible 9-track digital magnetic tapes for analysis by software realizations of several processing algorithms. By operating on recorded data from the radar data base, a valid comparison was possible by replaying flight test data, as opposed to conducting several live tests for the different processors. Figure 4 shows the equipment configuration for the data collection activity. The upper part of the diagram shows the on-line system that recorded data onto the high bit rate (HBR) instrumentation recorder, while the lower part shows the off-line data processing used to transfer sections of data to 6250 bpi 9-track magnetic tapes.

The on-line system used to gather data was the existing Signal Processing Laboratory (SPL) S-Band radar system with the HBR recorder interfaced to the receiver outputs. The S-Band antenna was controlled by hardware range and angle trackers. The transmit section consisted of the SPL waveform generator driving the S-Band exciter, the vertical and horizontal transmitters, and the transmit polarization controller.

The waveform generator produced a linear frequency modulated (LFM) waveform that was applied to both transmit channels simultaneously. The transmit polarization controller operated the transmitters sequentially so that interleaved horizontally and vertically polarized pulses were produced.

The receive section included the duplexers, receivers, low-pass filters, and analog to digital converters for the vertical and horizontal channels. The converter outputs were formatted by the 2:1 multiplexer for input to the HBR recorder. This machine recorded A/D data at a complex word rate of 4 MHz continuously in real time.

Radar parameters used for all experiments were as follows:

Operating frequency	3.35 GHz
Peak output power	150KW, nominal
Transmit PRI	2 milliseconds
Waveform type	Linear FM
Waveform bandwidth	2 MHz
Pulse duration	32 microseconds
Pulse compression ratio	64 to 1
A/D converter resolution	12 bits
A/D converter sample rate	2 MHz

The off-line system retrieved data from the HBR tape and transferred sections to hard disk on an HP A900 computer in the SPL, then to VAX-compatible 9-track tape. The intermediate transfer to disk storage was required to keep pace with the high playback data rate of the HBR recorder. The resulting 9-track tapes could then be processed with no limitations on algorithm complexity and computation times.

The procedure used to perform the data collection activity was as follows:

- a. Configure the dual-polarized S-Band radar to transmit interleaved horizontally and vertically polarized LFM pulses while receiving both polarization channels simultaneously.
- b. Calibrate the radar in order to achieve a match between the horizontal and vertical receive channels in magnitude and phase. Independently match the H and V transmit channels in magnitude and phase.
- c. Engage the acquisition radar system to locate targets and clutter areas of interest. The azimuth and elevation readings initialized and cued the S-Band antenna tracker.
- d. While tracking, record several minutes of the radar data onto the HBR tape recorder.
- e. Transfer several thousand PRI records of receiver data from the HBR tape to VAX-compatible 9-track tape via hard disk on the HP A900.

3.2 DATA REDUCTION

The primary function of the data reduction activity was to interface between the raw A/D converter outputs recorded on tape and the processor evaluation software. The processor evaluation was based on exploiting the different polarization and doppler characteristics of the target and clutter under analysis. These characteristics were contained in a set of six covariance sequences, as outlined below, derived from a particular section of raw data by the data reduction procedure and placed in a FORTRAN data file. Data reduction was performed on a number of sections of recorded returns to yield a collection of covariance sequence files. During the processor evaluation activity, these files were used as inputs to the software that calculated PD curves for the processors of interest. Three examples are presented in Figure 5.

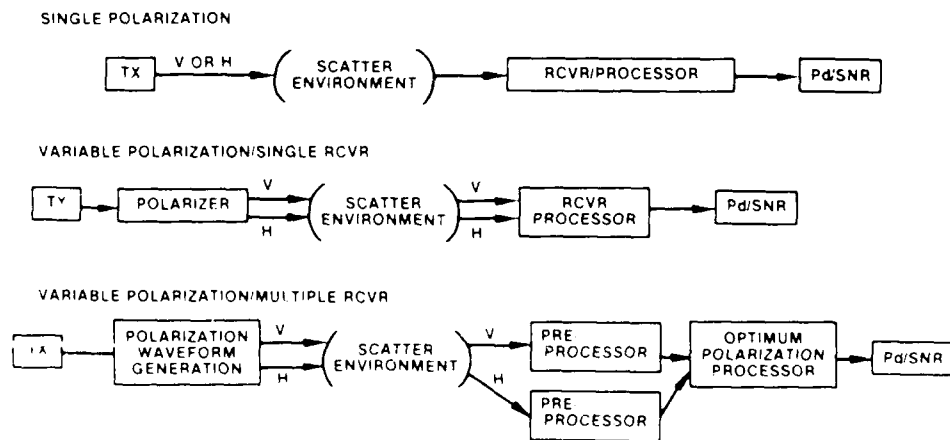


Figure 5. Three Polarization Receivers/Processors

A second function of data reduction was to provide additional information for judging the quality of the return data. Normally, a section of contiguous pulses was processed from the digital tape at one time. The data reduction software produced compressed-pulse plots of the horizontal and vertical return magnitudes versus range cell for the first pulse in the selected section. All pulses in the section were then pulse-compressed. A particular range cell of interest was chosen for analysis and the pulse compressor output values for this range cell in each return pulse were stored for subsequent processing. The data reduction software printed these peak values in a table and plotted their magnitudes.

The third function of the data reduction activity was to calculate and print out vector autoregressive model coefficients for the process generating the return.

3.3 PROCESSING ALGORITHMS

The process used for calculating the covariance sequences began by reading in and formatting the digitized radar samples from 9-track tape. The radar transmit schedule was chosen during data collection such that alternating horizontal and vertical pulses were transmitted. The receive system recorded two independent polarization channels simultaneously on each PRI. When a horizontal pulse was transmitted, two receive signals were captured, designated the horizontal transmit/horizontal receive (HH), and the horizontal transmit/vertical receive (HV) returns. During the next PRI, a vertical pulse was transmitted, and the two receive channels captured the vertical transmit/horizontal receive (VH), and the vertical transmit/vertical receive (VV) returns. The data formatting consisted of sorting these four types of returns into separate data streams.

The return pulses were pulse-compressed with a time-bandwidth product of 64. This was done in software using a two-transform technique with 35 dB Taylor weighting for

time sidelobe suppression.

The six covariance sequences generated were:

$$R_{HH,HH}(n) = E\{HH(i) HH^*(i+n)\}, \quad 1 \leq i \leq N \quad (41)$$

$$R_{VV,VV}(n) = E\{VV(i) VV^*(i+n)\}, \quad 1 \leq i \leq N \quad (42)$$

$$R_{HV,HV}(n) = E\{HV(i) HV^*(i+n)\}, \quad 1 \leq i \leq N \quad (43)$$

$$R_{HH,VV}(n) = E\{HH(i) VV^*(i+n)\}, \quad 1 \leq i \leq N \quad (44)$$

$$R_{HH,HV}(n) = E\{HH(i) HV^*(i+n)\}, \quad 1 \leq i \leq N \quad (45)$$

$$R_{VV,HV}(n) = E\{VV(i) HV^*(i+n)\}, \quad 1 \leq i \leq N \quad (46)$$

where $R(n)$ is the complex covariance sequence with the lag index n , $E\{\cdot\}$ is the expected value operator, and $*$ is the complex conjugation operator. N is the number of pulses processed. The arrays HH , VV , and HV contain the complex values of the compressed pulses at the particular range cell selected for processing.

The cross-polarization data array was formed by interleaving compressed pulse values at a single range cell from the HV and VH data streams. This represents the array of all cross-polarized returns from the chosen range cell. For a 64-pulse window, there were 32 HV returns, and 32 VH returns. The compressed pulse values from each range cell of interest were put into the HV array so that the first element was an HV sample, the second element a VH sample, etc.

The HH and VV arrays were formed differently from the cross-pol array because each has only one-half the number of samples as the interleaved HV/VH array. The samples filled the odd indexed elements of the HH array. The VV array was filled so that the even indexed elements contained the sample data. Since there were only one-half as many observations of the co-polarized returns as that of the cross-polarized returns, the values in

the HH and VV arrays were interpolated. The result was a set of three arrays, one containing cross-polarized observations, one containing HH observations, and one containing the VV observations. The cross-pol and interpolated HH and VV arrays each contained values representing observations at intervals of one PRI. All the arrays contained the same number of elements, equal to the number of PRIs in the pulse window to be processed.

The covariance sequences were estimated from these arrays. This was accomplished using a 4096 point Fast Fourier Transform and the results normalized to zero doppler frequency before the estimates were made. The samples were shifted so that the doppler peak was moved to the first sample. The location was determined by a magnitude peak search. Doppler normalization was required for the target because the processor evaluation software required target data at zero doppler frequency. Normalization was not performed on the clutter data.

The covariance sequences were computed for all six combinations of the HH, VV, and HV sample streams. They carried the doppler and polarization characterization of the target/clutter needed for use by the processor evaluation algorithms.

Given the experimentally derived covariance functions for each of the scattering matrix elements, the stochastic vector $h(t)$ was formed by modeling the data via a complex vector autoregressive process. The scattering model thus obtained provided the basis for the Optimum Matrix Method design. This allowed higher resolution estimates to be performed on limited observation data, enhancing performance.

An M^{th} order autoregressive process modeling the stochastic vector $h(t)$ is defined as follows:

$$\tilde{h}(t) = \sum_{k=1}^M [\tilde{A}_k \tilde{h}(t-kT) + \tilde{u}(t)] \quad (47)$$

where

\tilde{A}_k = 3x3 matrix of complex coefficients to be determined

$\tilde{h}(t)$ = 3x1 complex vector of covariance sequences

$$= \begin{bmatrix} \tilde{h}_{HH}(t) \\ \tilde{h}_{HV}(t) \\ \tilde{h}_{VV}(t) \end{bmatrix}$$

$\tilde{u}(t)$ = 3x1 complex, zero-mean white Gaussian noise vector

T = Sampling period (radar PRI)

M = Order of AR model

The \tilde{A}_k matrices are obtained by solving the Yule-Walker equations

$$\tilde{K}(mT) = \sum_{k=1}^M \tilde{A}_k \tilde{K}[(m-k)T] \quad m = 1, 2, 3, \dots, M \quad (48)$$

where

$$\begin{aligned} \tilde{K}(mT) &= 3 \times 3 \text{ complex covariance matrix} \\ &= E\{ \tilde{h}(t) \tilde{h}^*(t+mT) \} \end{aligned} \quad (49)$$

The M autoregressive model coefficient matrices are determined by solving equation (48) M times. The \tilde{K} matrices are determined by the data reduction procedure:

$$\tilde{K}(mT) = \begin{bmatrix} R_{HH,HH}(m) & R_{HH,HV}(m) & R_{HH,VV}(m) \\ R_{HH,HV}(m) & R_{HV,HV}(m) & R_{VV,HV}(m) \\ R_{HH,VV}(m) & R_{VV,HV}(m) & R_{VV,VV}(m) \end{bmatrix} \quad (50)$$

These are the tensor covariance elements of the scattering matrix developed in the theoretical discussion of the previous section with the assumption that the scatterers are isotropic, that is, $b_{VH} = b_{HV}$.

3.4 PROCESSOR EVALUATION

Five different processing algorithms were implemented in software and are briefly described here.

The Optimum Matrix Method (OMM) is shown in block diagram form in Figure 6. The processor consists of a weighting matrix followed by a maximum likelihood receiver. The inputs to this processor are the target and clutter samples of the scattering matrix. The first section of the processing program computes the optimum transmit waveform and the receive weighting/transform matrix. The second part of the program consists of an iteration loop wherein the target and clutter samples are processed by an optimum receiver. This includes transmitting the optimum waveform, operating on the return with the weighting/transform matrix, and comparing the result with a threshold. The number of threshold crossings is then counted and used in determining detection performance. A block diagram of the vector weighting method is shown in Figure 7. The method consists of two parts. The first includes an iterative loop to calculate the optimum weighting vector then a computation of the signal-to-clutter ratio resulting from the application of this optimum vector. The second part computes the signal-to-clutter ratio for the simple matched filter case. Plots of the outputs provide comparison of the optimum vector approach to the conventional matched filter method.

The dual adaptive processor used for evaluation of the optimum matrix method is described in reference [5]. It is implemented in two forms. The first is the original form, in which both transmit and receive polarizations are adaptive to any orientation. The second, designated the constrained optimum matrix method (COMM) processor, can adapt the transmit polarization only to one of sixteen discrete polarization orientations.

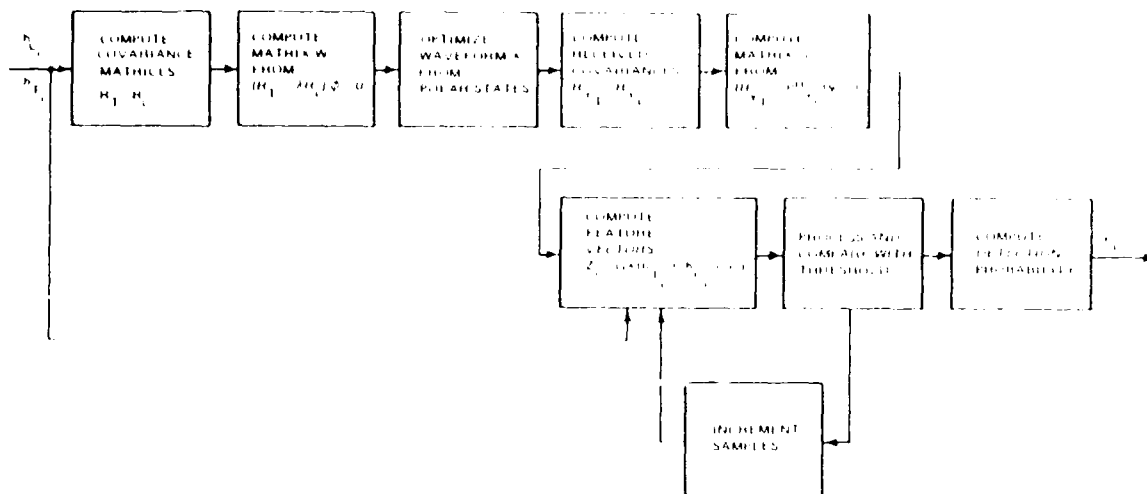


Figure 6. Optimum Matrix Method Processing Algorithm

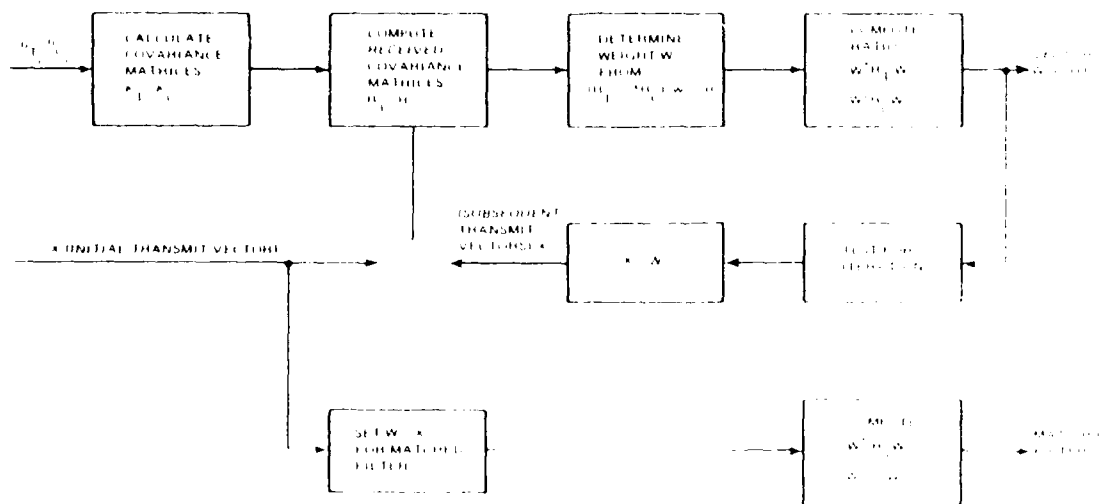


Figure 7. Block Diagram of Vector Weighting Simulation

The next technique considered was a receive-adaptive only processor implemented as a cascade of a normal adaptive doppler processor and a receive-adaptive polarization processor. This method transmits either horizontal or vertical fixed polarization, while its receive polarization adapts to minimize the clutter power. The doppler processing is optimum.

A fixed-polarization doppler processor is included for reference purposes. This method represents a system in which both the transmit and receive polarization orientations are either horizontal or vertical. Again, the doppler processing is optimum.

Finally, a noncoherent processor is implemented, also for reference. Both the transmit and receive polarization orientations are either fixed horizontal or fixed vertical.

A key to the curves on the PD plots identifying the processors associated with them is given in Table 1.

TABLE 1. Key to Curves on PD Plots

<u>Curve</u>	<u>Transmit polarization</u>	<u>Receive polarization</u>	<u>Doppler filtering</u>	<u>Characteristics</u>
1	Pulse-to-pulse adaptive	Pulse-to-pulse adaptive	Adaptive, optimum	Optimum Matrix Method
2	Fixed	Adaptive	Adaptive, optimum	Receive polarization adapts to minimize clutter power
3	Fixed	Fixed	Adaptive, optimum	No polarization adaptivity
4	Fixed	Fixed	None	Noncoherent pulse summation
5	Pulse-to pulse adaptive, constrained	Pulse-to-pulse adaptive	Adaptive, optimum	Constrained OMM

The processor evaluation software produced probability of detection (PD) curves using recorded target/clutter data. PD plots were also created for simulated targets to predict radar performance under conditions for which no recorded data was available. In cases that used simulated target or clutter inputs, the program was given the appropriate parameters. For simulated targets the following parameters were specified:

a. Angle – This is the primary orientation of the target scatterer. Possible values are horizontal, 45° linear, and vertical.

b. Angle Spread – This is the standard deviation of the angle of the target with respect to its mean angle, in radians.

c. Doppler Spread – This is the standard deviation of the target doppler frequency, as a decimal fraction of the pulse repetition frequency (PRF). The software requires all targets to be at zero mean doppler frequency.

The parameters that were selected in the clutter simulation are:

a. Angle – This is the primary orientation of the clutter polarization. Possible values are horizontal, 45° linear, and vertical.

b. Angle Spread – This is the standard deviation of the clutter polarization angle with respect to its mean angle, in radians.

c. Doppler Mean – This is the mean clutter doppler frequency as a decimal fraction of the PRF.

d. Doppler Spread – This is the standard deviation of the clutter doppler frequency, as a decimal fraction of the PRF.

These parameters were chosen for each example to correspond to a reasonable model for an aircraft target, ground and rain clutter, or chaff, as needed for the simulation input. The output of these test cases are displayed in plots of PD versus

SNR for three clutter-to-noise ratios (CNR). The CNRs were -20dB, +10dB, and +30dB. The complete set of results is available for several sets of recorded and simulated data. The data plots presented here represent the case of recorded target/recorded ground clutter with the following target parameters:

Angle	= horizontal
Angle Spread	= 0.2
Doppler freq	= 0 (normalized)
Doppler Spread	= 0.02

Similar parameters apply for the recorded ground clutter. Figures 8 to 13 show the results of the processor evaluation for the three clutter to noise ratios considered. Figure 14 is a plot of the compressed target data used in this example when transmitting and receiving horizontal polarization. The target is at 36 nautical miles in range and is 25 dB above noise and sidelobe components. Figure 15 is a plot of the pulse compressed ground clutter data used in the example. In this case, the clutter was approximately 20 dB stronger than the target. Figure 16 is a plot of the pulse compressed target when the transmitted waveform was horizontal and the received waveform was vertical. The signal was down approximately 17 dB from the HH case considered previously. Figure 17 is a plot of the pulse compressed clutter data resulting from horizontal transmit and vertical receive polarizations. The clutter in this case is approximately 15 dB weaker than the HH case. Figures 18 and 19 are the target and clutter spectra for the cross polarized, horizontal transmit and vertical receive combination.

The OMM and COMM processors showed superior detection results over the other processors for this data set, as in all the cases evaluated.

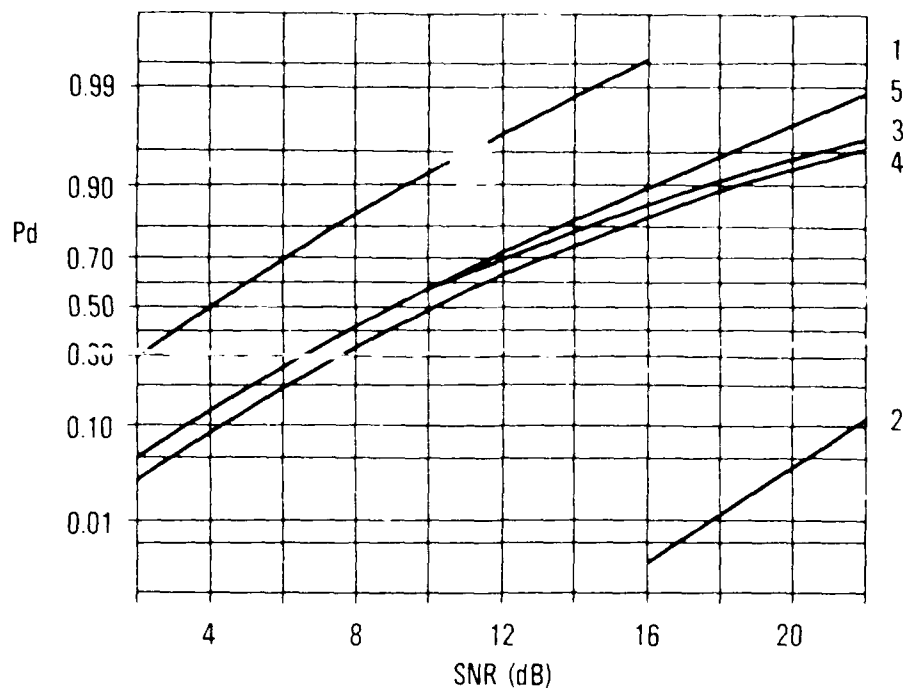


Figure 8. Horizontal Transmit Polarization, CNR = -20dB

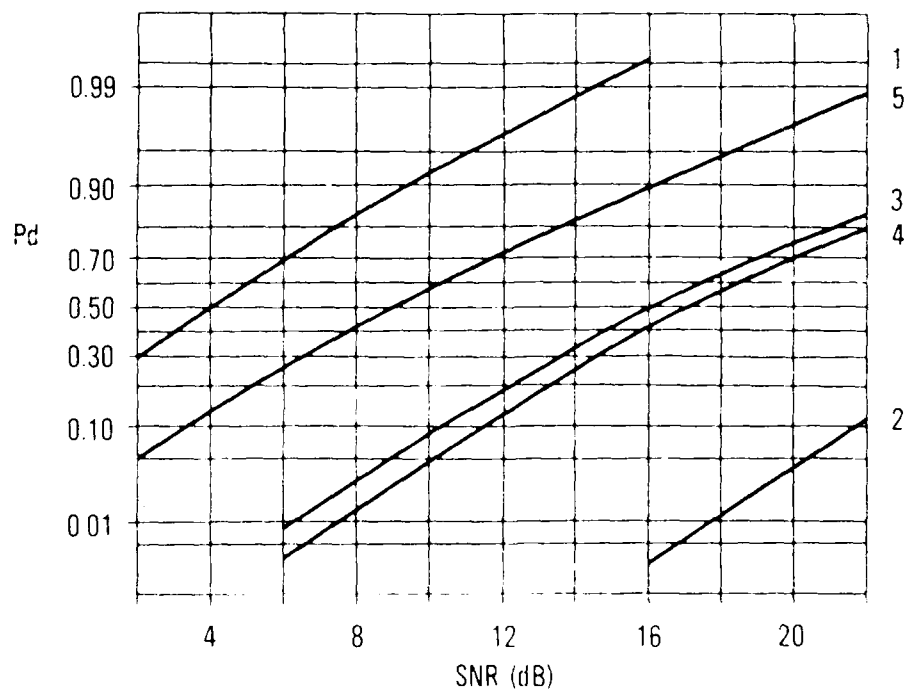


Figure 9. Vertical Transmit Polarization, CNR = -20dB

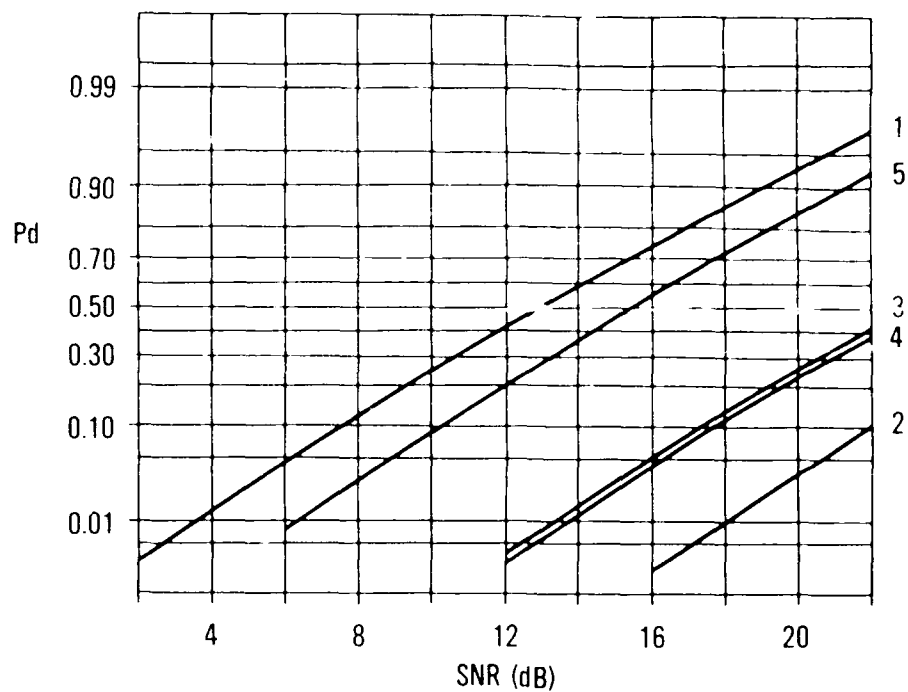


Figure 10. Horizontal Transmit Polarization, CNR = 10dB

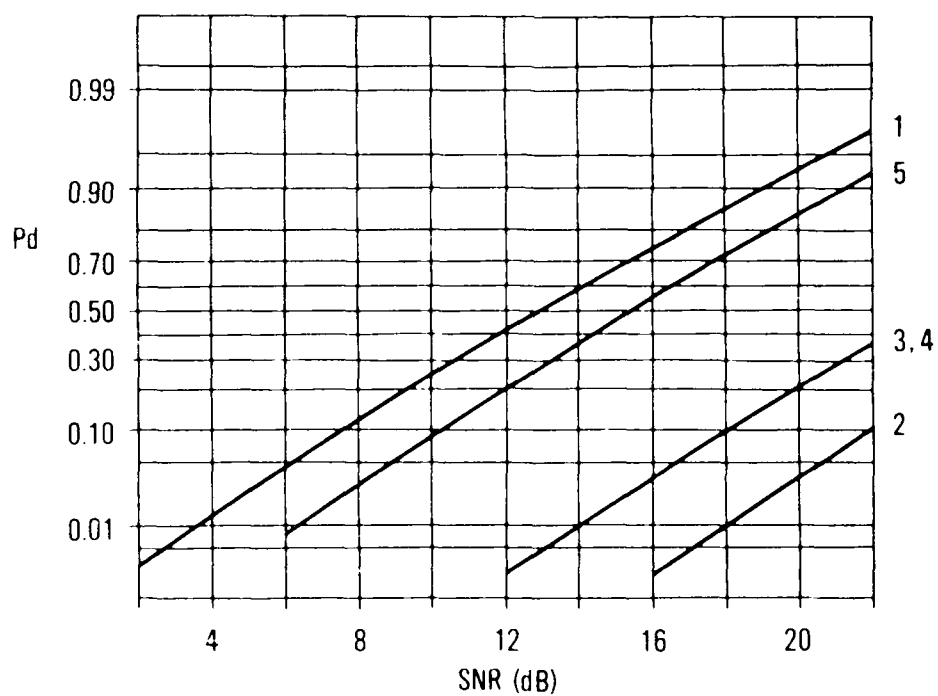


Figure 11. Vertical Transmit Polarization, CNR = 10dB

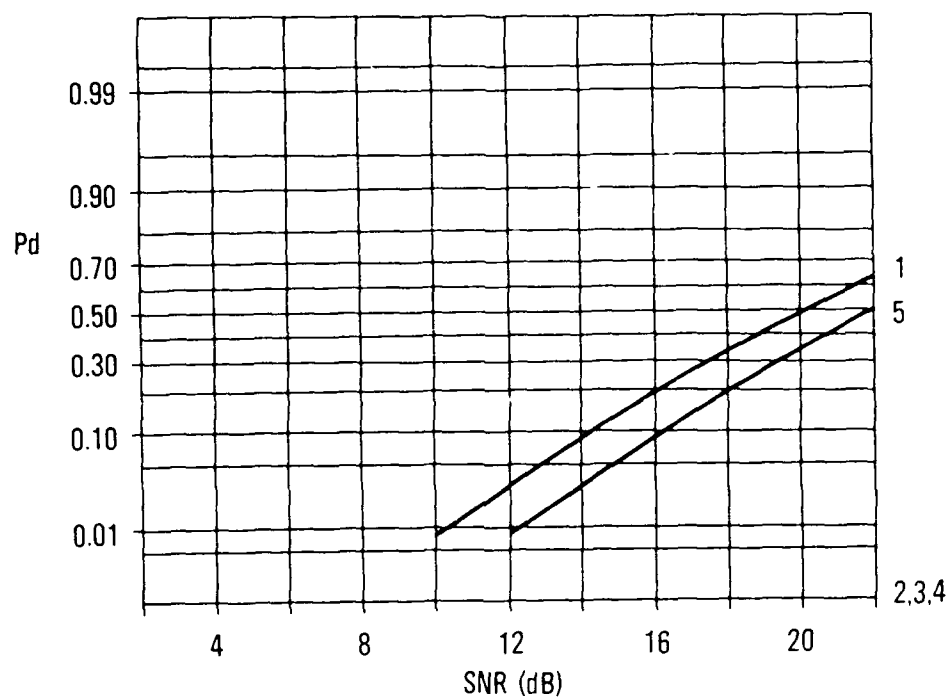


Figure 12. Horizontal Transmit Polarization, CNR = 30dB

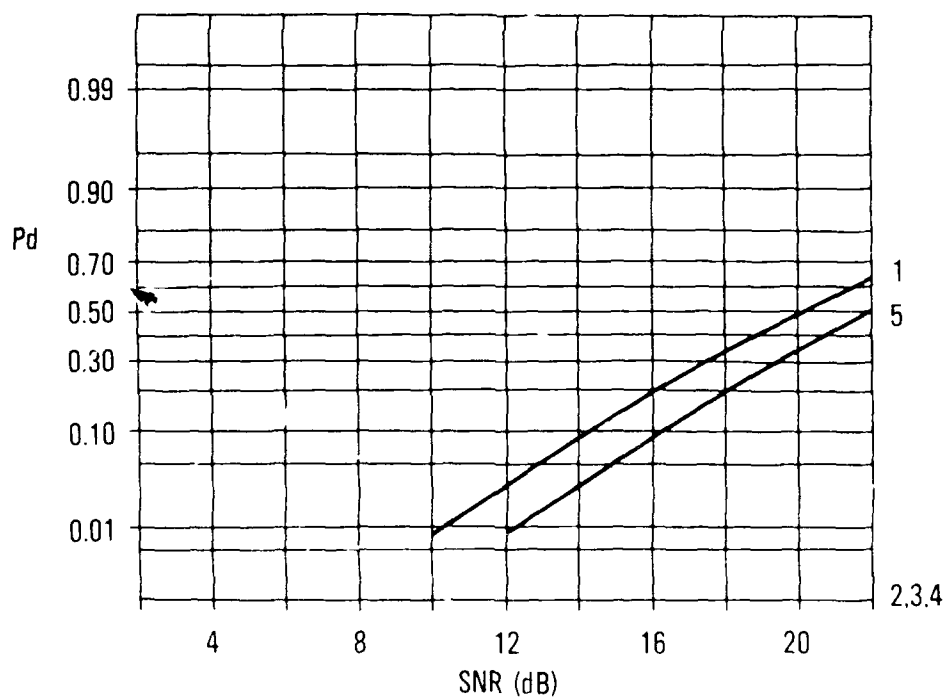


Figure 13. Vertical Transmit Polarization, CNR = 30dB

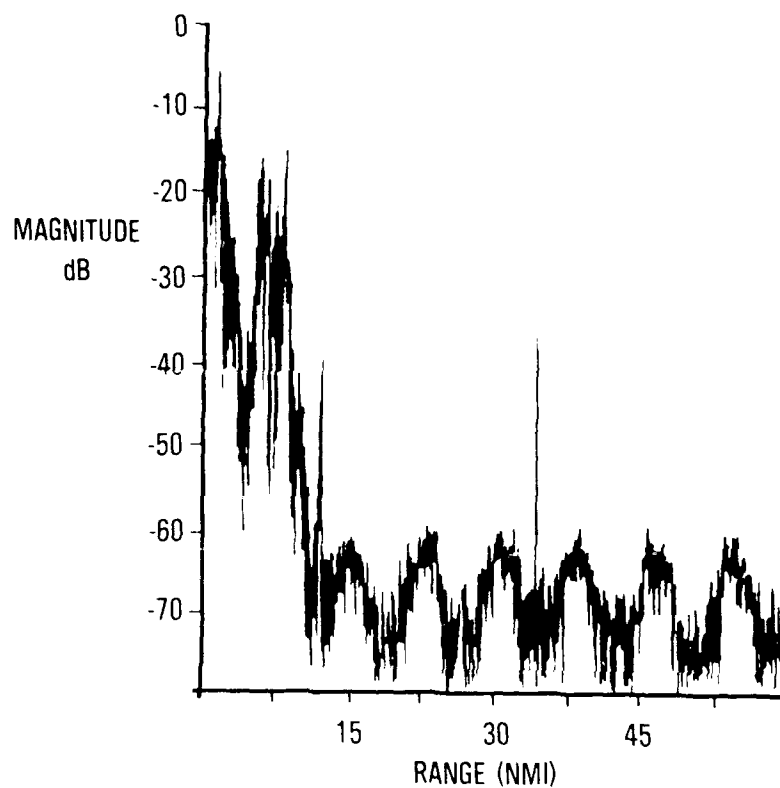


Figure 14. Pulse Compressed Target Data (HH)

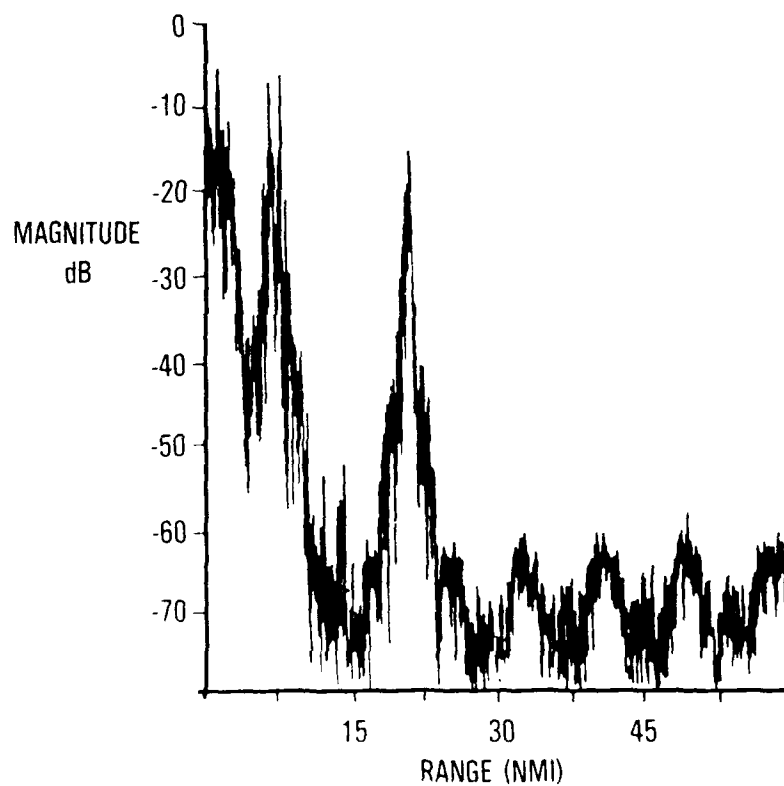


Figure 15. Pulse Compressed Clutter Data (HH)

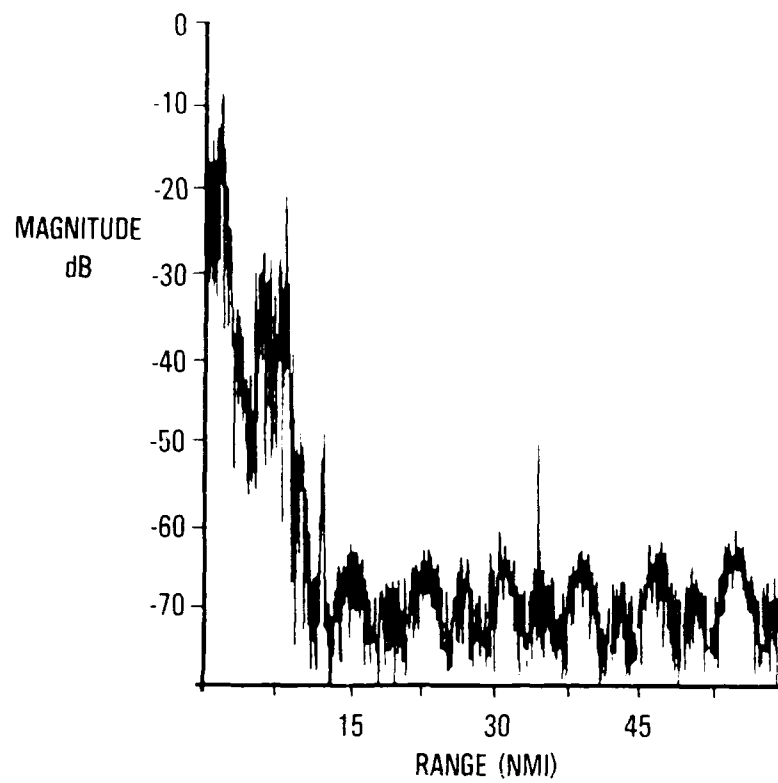


Figure 16. Pulse Compressed Target Data (HV)

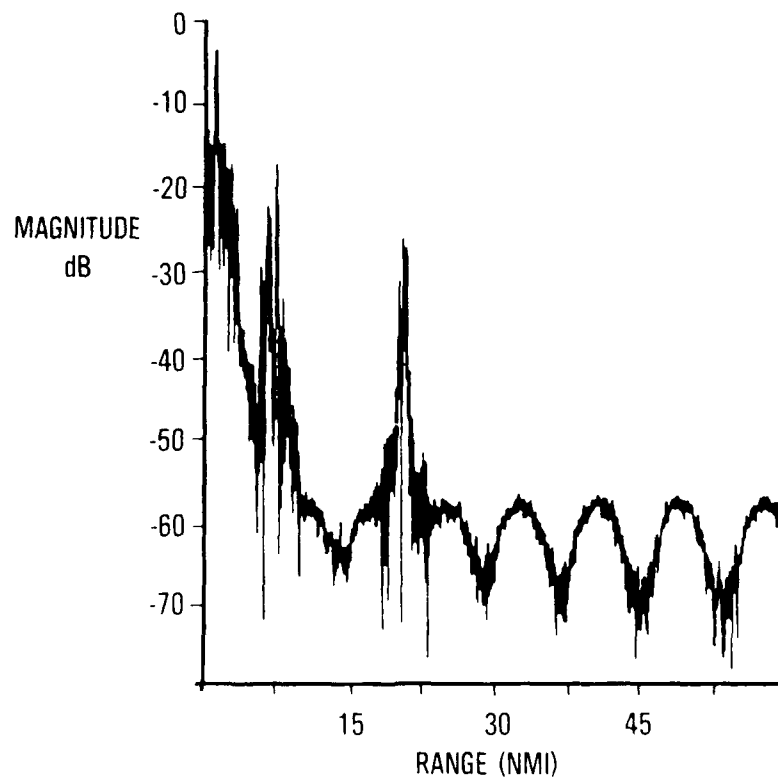


Figure 17. Pulse Compressed Clutter Data (HV)

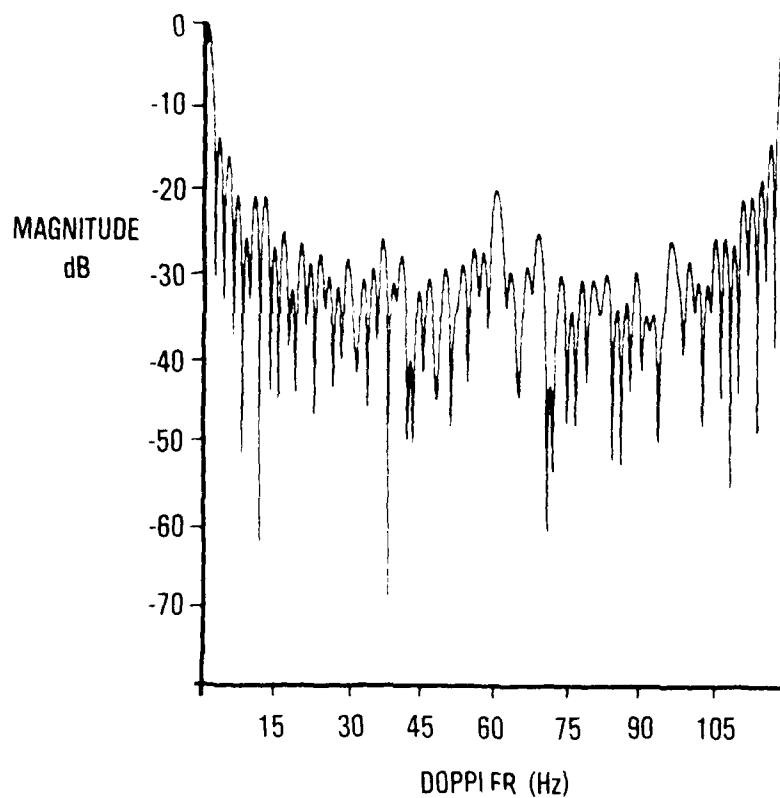


Figure 18. Target Spectrum (HV)

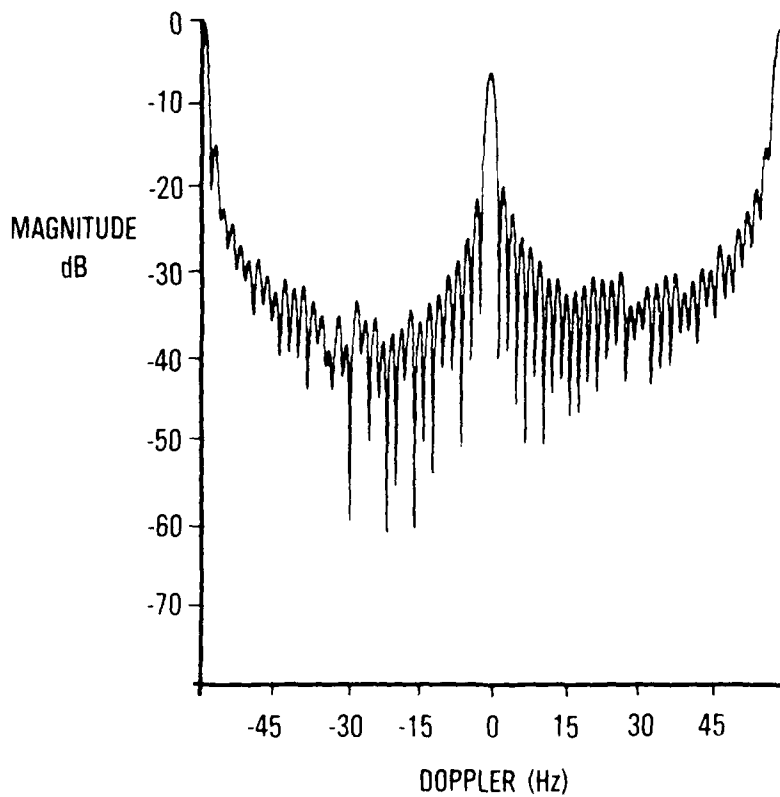


Figure 19. Clutter Spectrum (HV)

4.0 EXPERIMENTAL RESULTS

In this section, the results of recent RADC polarization processor evaluation experiments are presented. Actual flight test data provided improved confidence in the evaluation compared to simulated data, and resulted in a library of fundamental measurements of the doppler and polarization properties of targets and chaff.

The data collection, reduction, and processor evaluation were performed as previously described, but results were plotted in several different forms. Included here are raw data, pulse compressed data, and spectral analyses of HH, HV, VH, and VV components. In the previous section, the target and clutter data were combined in the pre-processing algorithm for subsequent evaluation. In this section, we present a three dimensional range-doppler plot of target and chaff from the same data recording.

The chaff drop took place in the vicinity of Griffiss AFB, New York, in May 1988, using chaff cut specifically to enhance reflections at S-Band. The target was a medium size aircraft which flew above the chaff cloud. The digitized receiver outputs were recorded during the chaff drop, and processed off-line after the flight. This experimental mode provides two principal advantages. First, the same series of flight test data was replayed for processing by each algorithm, to insure a valid comparison. Second, processing algorithms to be evaluated could be arbitrarily complex since they were relieved of the requirement to operate in real time. Hardware pulse compression was available for rapid location of targets during the test. This was invaluable for locating targets in the mass of recorded data during high speed playback. The algorithms employed software pulse compression with floating point Fast Fourier Transform (FFT) computations to achieve maximum dynamic range, once the critical data segments had been located.

Figure 20 is a plot of uncompressed data showing the co-polarization and

cross-polarization components from successive interleaved transmit pulses. The transmit sequence allowed the four scattering matrix components to be observed every two pulses. The first pulse transmitted was vertically polarized, with both vertical and horizontal receive data recorded. The next pulse transmitted was horizontally polarized, with both vertical and horizontal returns recorded simultaneously. The plot represents a range extent of 40 nautical miles, 4 miles per division, and a linear amplitude scale. The target can be seen in the VV plot at approximately 12 nautical miles, about 4 miles before the edge of the chaff cloud. The target also appears in the remaining three plots, but at a reduced amplitude relative to the background level. The chaff return is maximum in the HH channel, but has substantial components on all plots, presumably due to atmospheric turbulence. The signal components of VH and HV are nearly equal. Thermal noise is independent between these channels, however, and is slightly greater in the vertical receive channel.

Figure 21 shows data taken approximately three seconds after the data shown in Figure 20. The fine structure of the plots are somewhat different, but the signal components have nearly the same properties as before. The chaff structure changes continuously due to varying dipole orientation as affected by the their fall rate and wind velocity. Figures 22 and 23 are plots of the compressed pulse showing both the target and the chaff for both of the above cases. The experimental work described in this paper was performed in two stages. The first effort, reported in reference [9] included eight evaluations using various combinations of simulated and recorded targets and clutter data to illustrate detection characteristics of the processors operating both in thermal noise and against clutter. Recorded ground clutter, rain clutter, and aircraft target data were used. Simulated data used in stage one included aircraft targets, ground clutter and chaff.

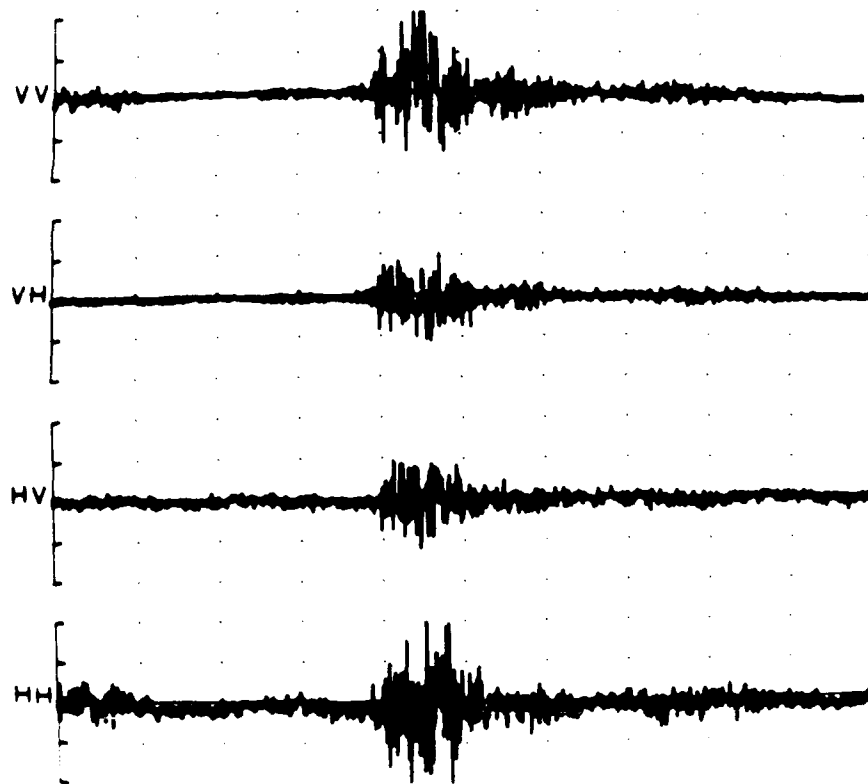


Figure 20. Uncompressed Target and Clutter Data
I Channel versus Range

The second stage of the experiment, conducted in-house included an upgrade of the S-Band radar sensor and adaptive calibration of the receiver channels to obtain equal HV and VH returns. The data analyzed in this stage was from an actual chaff drop with an aircraft test target.

In the first stage, the performance of the candidate processors was evaluated for several cases including all combinations of recorded and simulated clutter and target data. The processors that were evaluated include a fixed-polarization noncoherent integrator, a fixed-polarization receive-adaptive doppler filter bank, the Optimum Matrix Method

(OMM), and a Constrained Optimum Matrix Method (COMM) processor. The algorithms were compared by examining PD curves versus SNR and measuring the relative performance of the processors expressed in dB.

The fixed polarization noncoherent integrator was used as the basis for comparison with the other processors. Probability of detection values up to 0.7 were obtained for the $\text{CNR} = -20$ dB (thermal noise only) cases in which the transmitted polarization coincided with the orientation of the target. PD values were dramatically lower for the same processor implemented with transmitted polarization orthogonal to the target. Cases using recorded target and recorded clutter indicated that a 12 dB higher signal level is required

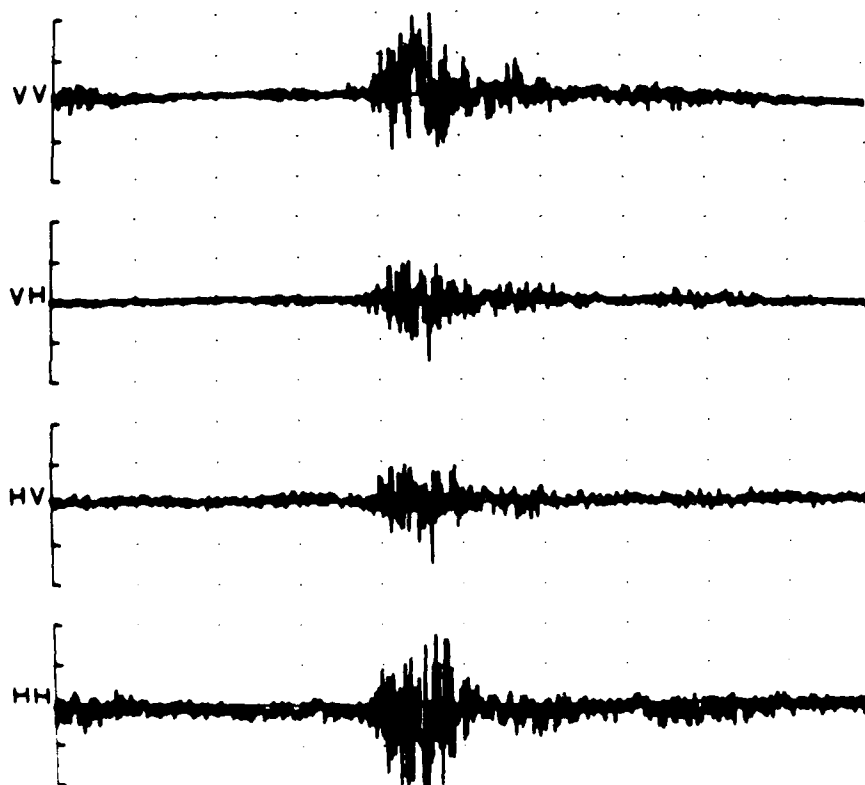


Figure 21. Uncompressed Target and Clutter Data

3 second delay from Fig 20

to achieve the same PD when the CNR is increased from -20 dB to +10 dB. Probability of detection approached zero for all cases where $\text{CNR} = +30 \text{ dB}$.

The fixed-polarization doppler processor models a radar in which transmit and receive channels have the same polarization, and uses optimum doppler processing. This processor performed better than the noncoherent integrator. Probability of detection was improved over the noncoherent integrator for the $\text{CNR} = -20 \text{ dB}$ (thermal noise only) cases in which the transmitted polarization coincided with the orientation of the target. PD values were dramatically lower for the processor implemented with transmitted polarization orthogonal to the target. Cases using recorded target and clutter indicated that an 11 dB higher signal level is required to achieve the same PD, when the CNR is increased from -20 dB to +10 dB. Probability of detection approached zero for all cases where the interference was strong ($\text{CNR} = +30 \text{ dB}$).

The fixed-polarization processor represents the conventional doppler radar which uses the same linear polarization for both transmit and receive antennas. The main cause of poor performance for this processor is its inability to illuminate targets whose primary scattering orientation is orthogonal to the radar receiving polarization.

The receive-adaptive processor exhibited the worst detection capability of all the processors. This implementation models a radar system that uses a fixed polarization transmit pulse, but adapts the receive polarization so that it is orthogonal to the clutter return. Doppler filtering is optimum.

To achieve equivalent detection performance, the receive-adaptive processor required an average of 17 dB higher signal level than the noncoherent integrator for a CNR of -20 dB, when the transmitted polarization coincided with the orientation of the target. Detection was impossible when the transmit polarization was orthogonal to a target with a small angular spread.

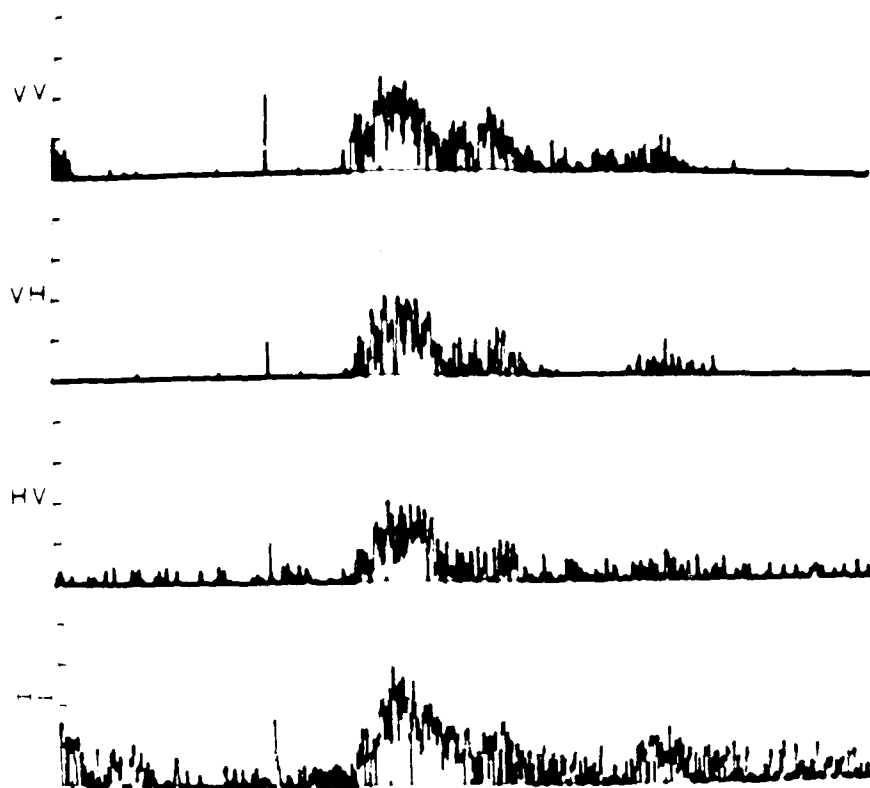


Figure 22. Pulse Compressed Target and Clutter Data
Magnitude versus Range

Probability of detection performance for the receive-adaptive processor ($\text{CNR} = +10$ dB) was from 2 to 9 dB poorer than for the noncoherent integrator. Probability of detection approached zero for all $\text{CNR} = +30$ dB cases.

The receive-adaptive processor represents a partially adaptive doppler radar which uses the polarization discriminant to achieve a receive polarization that nulls clutter returns. The experiments revealed a deficiency in this algorithm in that it sometimes severely attenuates the target along with the clutter. The effect was observed in all cases in

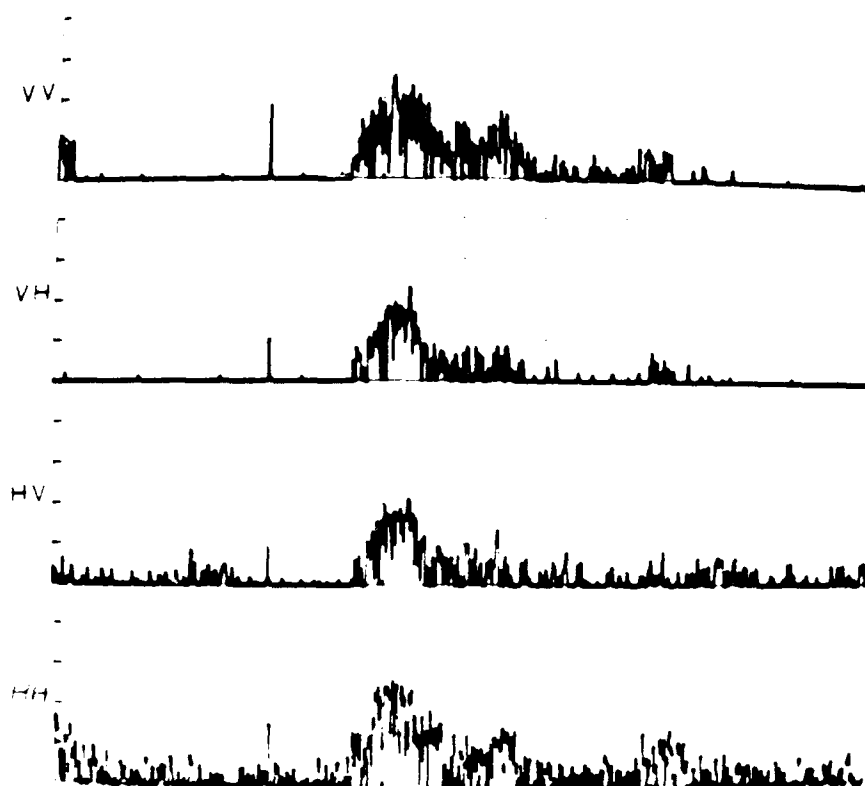


Figure 23. Pulse Compressed Target and Clutter Data

3 second delay from Fig 22

which the target and clutter had the same angular orientation. As with the other fixed-polarization processors, performance was also degraded by its inability to illuminate targets whose primary scattering orientation was orthogonal to the transmit polarization.

The OMM processor gave the best detection performance of all those evaluated. This processor models a radar system that is jointly adaptive in both doppler and polarization domains. The OMM processor performed 6 to 12 dB better than the noncoherent integrator in the recorded target/recorded clutter example for a CNR of -20 dB. PD values of 0.95 to 0.99 were obtained at a SNR of 12 dB in this example, compared with values of 0.05 to 0.55

for the noncoherent integrator. The OMM processor coped very well with rising levels of interfering clutter. For a 30 dB increase in CNR, from -20 dB to +10 dB, the OMM required an average increase of only 9 dB in signal level to preserve detection. Detection performance for the OMM processor was degraded only approximately 5 dB for CNR = +30 dB compared to that obtained for CNR = +10 dB using recorded targets and clutter.

Overall, the Optimum Matrix Method processor demonstrated far better probability of detection than the other processors, especially in severe clutter, where the non-optimal processors gave little or no detection capability.

The Constrained Optimum Matrix Method (COMM) processor demonstrated the second best detection performance of the processors tested. This processing algorithm is nearly identical to the OMM with the exception that the transmit polarization orientation is selected from one of 16 discrete angles, equally spaced from 0 to 360 degrees. This represents a simplified implementation of the OMM algorithm that would require less transmitting hardware complexity.

The COMM processor detection performance was an average of 6 dB worse than the OMM implementation in the recorded target/recorded clutter examples over all three CNR levels. This processor shows a 6 dB improvement over the noncoherent integrator.

The stage two effort featured the availability of actual chaff and target data for further processor evaluation. The range-doppler properties of the measured data are presented in Figure 24. The doppler processing method consisted of applying 40 dB Chebychev weights to multiple pulse data from each range index, then performing an FFT to obtain the doppler spectrum. The chaff appears highly spread in doppler, presumably due to atmospheric turbulence. At S-band, the doppler frequency is approximately 12 Hz per knot, and doppler ambiguities occur at multiples of the pulse repetition frequency. The target doppler is ambiguous on this plot, and has wrapped around several times.

The results of the chaff drop and target aircraft experiments carried out in the second stage of this effort show some differences in processor performance compared to the stage one results. See Figures 25 through 30. The fixed polarization, noncoherent integrator, had maximum performance when the transmitted polarization coincided with the target orientation. For the case where $\text{CNR} = -20$ dB, PD values up to 0.5 were observed. For cross polarized returns, PD decreased to 0.15. Increasing the CNR to +10 dB decreased the PD to 0.05 for co-polar and 0.005 for the cross-polar case. Probability of detection approaches zero for both orientations when $\text{CNR} = 30$ dB. These results show that the noncoherent integrator performed better in stage one (recorded target and ground clutter) than in stage two (recorded aircraft and chaff). The measured performance difference was 1.5 dB for the co-polar return and 0.5 dB for the cross-polar return.

As in the first stage, the fixed polarized doppler processor performed better than the noncoherent integrator. In the case of $\text{CNR} = -20$ dB, the observed PD was 0.55 for the co-polar return, and 0.30 for the cross-polar return. For the case of $\text{CNR} = 10$ dB, the PD became 0.25 for the co-polar return and 0.05 for the cross-polar return. PD dropped to zero for $\text{CNR} = +30$ dB. These results showed somewhat higher performance than the stage one results, i.e., 6 dB for the co-polar return and 4 dB for the cross-polar return, with $\text{CNR} = -20$ dB.

The fixed polarization processor achieved a PD of 0.65 for co-polar returns and 0.35 for the cross-polar returns for $\text{CNR} = -20$ dB. For $\text{CNR} = +10$ dB, PD was reduced to 0.25 for co-polar returns, and 0.05 for cross-polar returns, and at $\text{CNR} = +30$ dB, PD approached zero. As compared to stage one, these results show a decrease of 4 dB for copolar returns and an increase of 3 dB for the cross-polar returns when $\text{CNR} = -20$ dB.

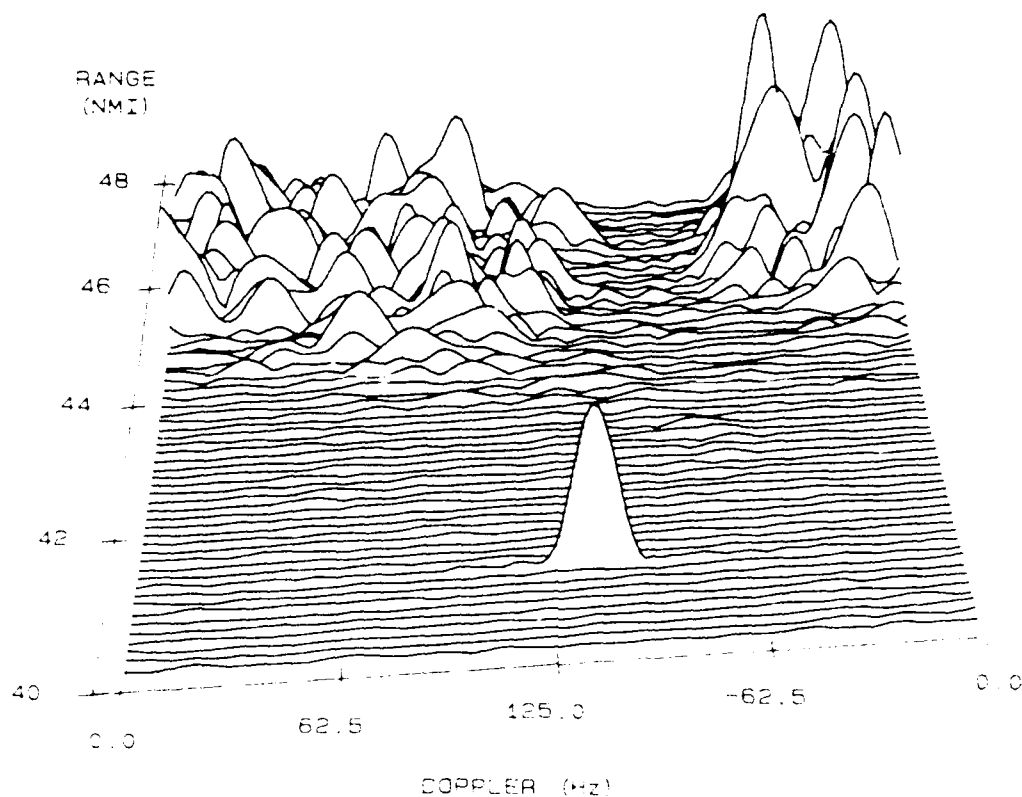


Figure 24. Range Doppler 3D Plot of Aircraft and Chaff

The receive-adaptive processor showed mixed results. While performance was poorer than the other processors with $\text{CNR} = -20$ dB, it was better than the noncoherent integrator and fixed polarization processor when $\text{CNR} = +10$ dB. The PD for $\text{CNR} = -20$ dB was 0.25 for co-polar returns and 0.15 for cross-polar returns. With $\text{CNR} = +10$ dB, PD became 0.15 for co-polar returns, and 0.075 for cross-polar returns, and for $\text{CNR} = +30$ dB, PD approached zero. These results represent an increase of more than 7 dB for both co-polar and cross-polar operation over stage one results, with $\text{CNR} = -20$ dB.

The OMM processor produced the best results, as observed in stage one. For $\text{CNR} = -20$ dB, a PD of 0.8 was obtained for co-polar returns, and 0.7 for cross-polar returns. With $\text{CNR} = +10$ dB, the PD became 0.55 for both co-polar and cross-polar returns. In the case of $\text{CNR} = +30$ dB, PD dropped to 0.001 for both co-polar and cross-polar returns. These results were 5 dB poorer than those observed in stage one, most likely due to the turbulent and noiselike nature of the chaff returns as compared with ground clutter. The COMM processor was second in performance to the OMM processor, as in stage one, achieving a PD of 0.45 for both co-polar and cross-polar returns with $\text{CNR} = +10$ dB.

Refer to Table 1 for a complete key to PD curves in Fig 25 - Fig 30.

In summary, the processor identification is:

- 1 - Optimum Matrix Method
- 2 - Receive-adaptive polarization
- 3 - Fixed polarization, optimum doppler
- 4 - Fixed polarization, noncoherent pulse summation
- 5 - Constrained Optimum Matrix Method

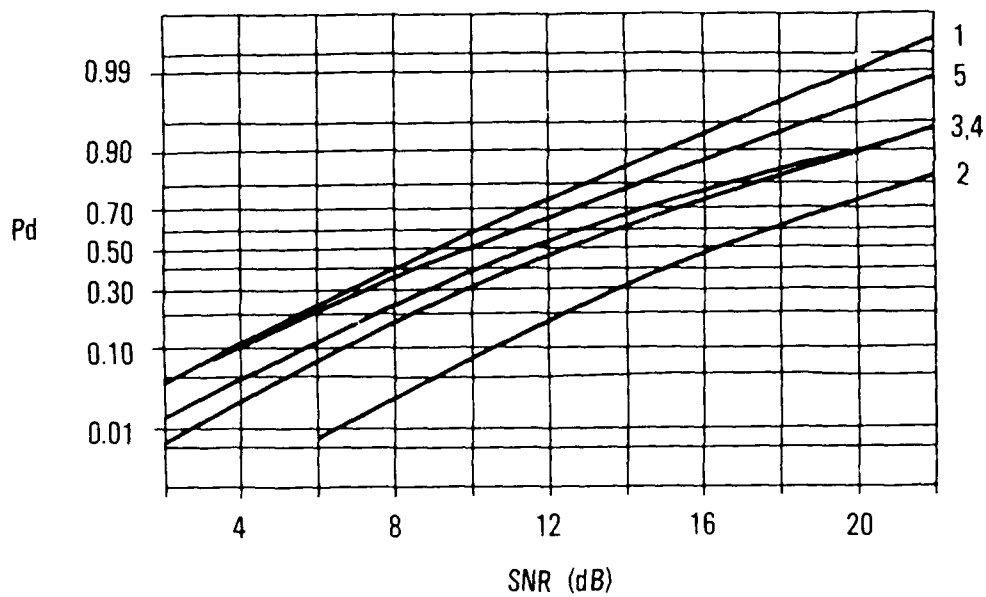


Figure 25. Horizontal Transmit Polarization, CNR = -20 dB

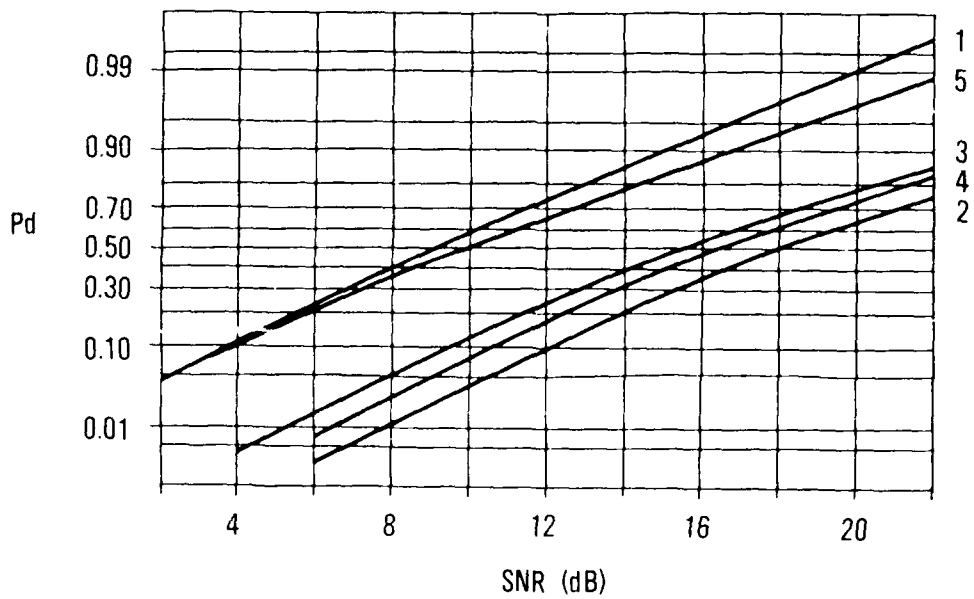


Figure 26. Vertical Transmit Polarization, CNR = -20 dB

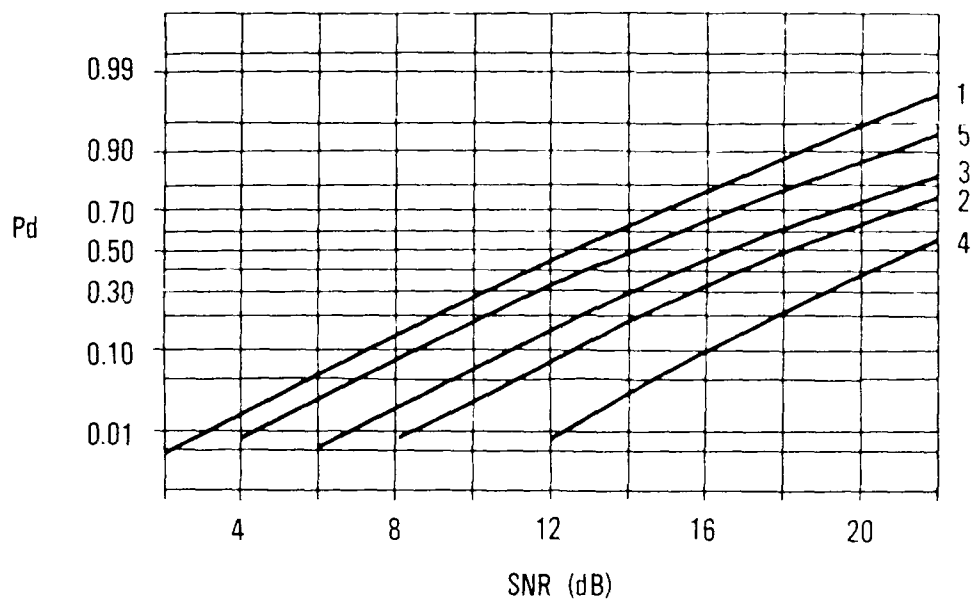


Figure 27. Horizontal Transmit Polarization, CNR = 10 dB

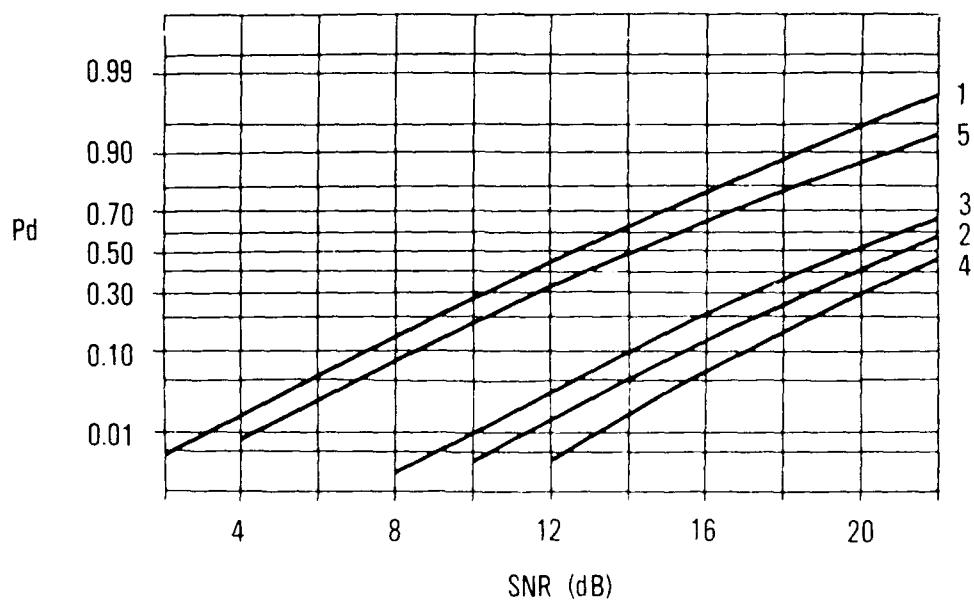


Figure 28. Vertical Transmit Polarization, CNR = 10 dB

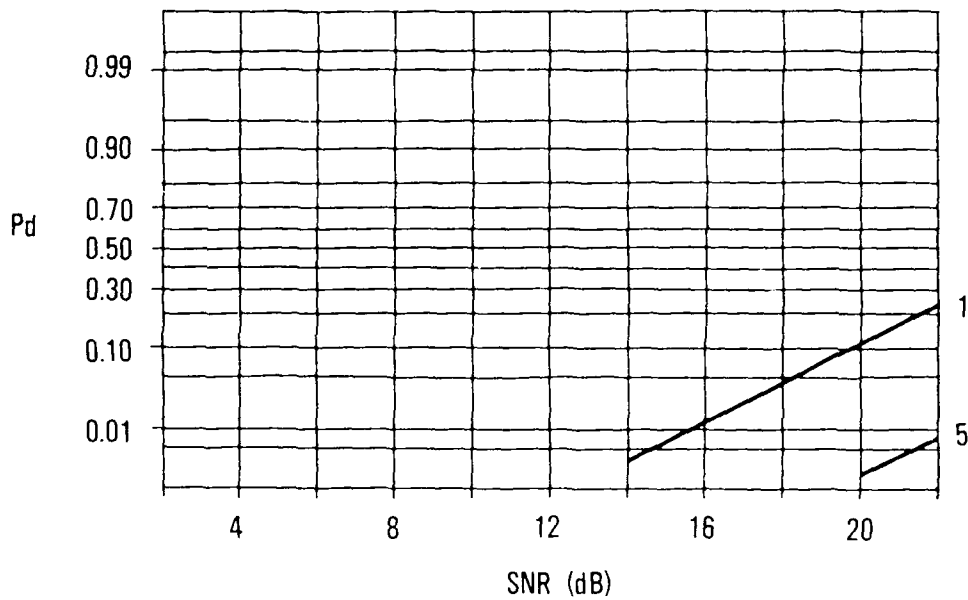


Figure 29. Horizontal Transmit Polarization, CNR = 30 dB

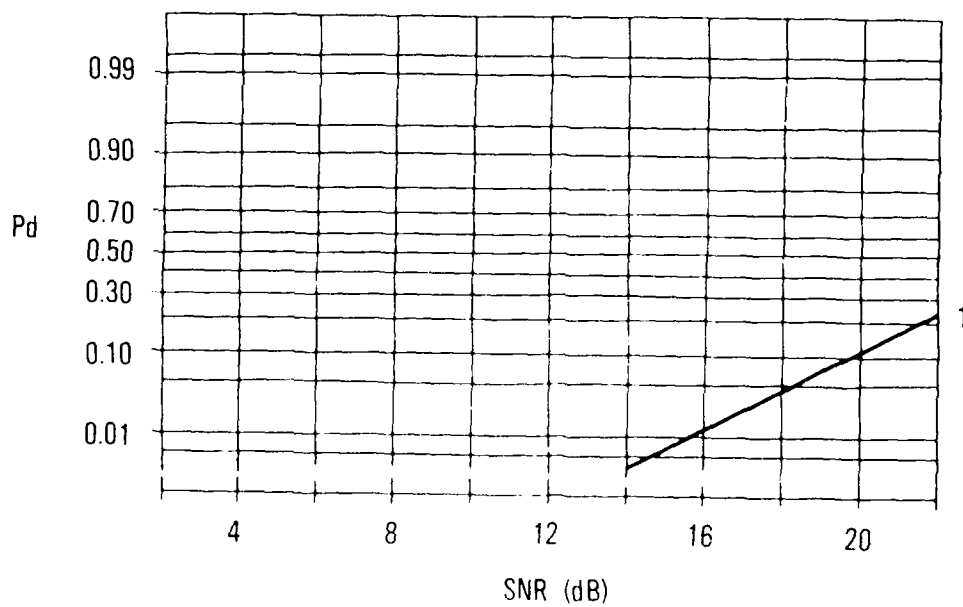


Figure 30. Vertical Transmit Polarization, CNR = 30 dB

5.0 CONCLUSIONS

The foregoing experimental results have demonstrated that adaptive coherent polarimetric radar techniques provide enhanced target detection in the presence of clutter and chaff. An analytic approach was developed for dual channel optimum processing of range-doppler spread targets and clutter. Matrix methods were utilized to develop and implement an optimal polarization diverse transmit waveform and optimum dual channel receiver, which maximize the signal-to-interference ratio and enhance target detection. This doubly adaptive approach, referred to as the Optimum Matrix Method (OMM), was shown experimentally to be superior to conventional radar processing techniques. A Constrained OMM, limited to one of sixteen fixed transmit polarizations was also evaluated and nearly approaches the performance of the fully adaptive system. Three conventional, fixed polarization radar systems were implemented and compared to the polarization diverse processors. The average performance improvement which could be attributed to adaptive polarization diversity was 6-10 dB for the Optimum Matrix Method and 4-6 dB for the Constrained OMM.

6.0 REFERENCES

- [1] Van Trees, H. L., "Detection, Estimation, and Modulation Theory, Part III", John Wiley & Sons, Inc., 1971.
- [2] Poelman, A. J., "Cross Correlation of Orthogonally Polarized Backscatter", IEEE AES-12, No. 6, pp 674-682
- [3] Varshanchuk, M. L. and Kobak, V. O., "Cross Correlation of Orthogonally Polarized Components of Electromagnetic Fields, Scattered by an Extended Object", Radio Eng. Electron Phys., Vol 16, pp 201-205, February 1971.
- [4] Ioannidis, G. A., "Model for Spectral and Polarization Characteristics of Chaff", IEEE AES-15, No. 5, pp 723-726, September 1979.
- [5] Rome Air Development Center, "Polarization Processing Techniques Study", Final Report, RADC-TR-79-285, November 1979, AD No. A080 565, Contract No. F30602-78-C-0119.
- [6] Fujita, M., and Klein A., "Adaptive Polarization Processing", Workshop on Polarimetric Radar Technology, U.S. Army Missile Command, Redstone Arsenal, 25-26 June 1980.

- [7] Vannicola, V.C. and Lis, S., "Polarization Vector Signal Processing for Radar Clutter Suppression", Inverse Methods in Electromagnetic Imaging, Part 2; NATO ASI Series C: Mathematical and Physical Sciences, 1983, Vol 143, pp 739 - 770.

- [8] Rome Air Development Center, "Signal - Filter Design and System for Polarimetric Radar", Final Technical Report, RADC-TR-87-3, July 1987, A189257, Contract No. F30602-84-C-0017.



MISSION of *Rome Air Development Center*

RADC plans and executes research, development, test and selected acquisition programs in support of Command, Control, Communications and Intelligence (C³I) activities. Technical and engineering support within areas of competence is provided to ESD Program Offices (POs) and other ESD elements to perform effective acquisition of C³I systems. The areas of technical competence include communications, command and control, battle management information processing, surveillance sensors, intelligence data collection and handling, solid state sciences, electromagnetics, and propagation, and electronic reliability/maintainability and compatibility.